Managing connected and automated vehicles with flexible routing at “lane-allocation-free” intersections

Hao, Ruochen; Zhang, Yuxiao; Ma, Wanjing; Yu, Chunhui; Sun, Tuo; van Arem, Bart

DOI
10.1016/j.trc.2023.104152

Publication date
2023

Document Version
Final published version

Published in
Transportation Research Part C: Emerging Technologies

Transportation Research Part C 152 (2023) 104152

Contents lists available at ScienceDirect

Transportation Research Part C

journal homepage: www.elsevier.com/locate/trc

Managing connected and automated vehicles with flexible routing at "lane-allocation-free" intersections

Ruochen Hao [a,b], Yuxiao Zhang [a], Wanjing Ma [a,*], Chunhui Yu [a,*], Tuo Sun [a], Bart van Arem [b]

[a] Key Laboratory of Road and Traffic Engineering of the Ministry of Education, Tongji University, 4800 Cao'an Road, Shanghai, PR China
[b] Department of Transport and Planning, Delft University of Technology, 2628 CN Delft, The Netherlands

ARTICLE INFO

Keywords:
Connected and automated vehicle
Isolated intersection
Lane-allocation-free
Signal-free
Flexible routing

ABSTRACT

With the development of internet of vehicles and automated driving, individual-based trajectory control at intersections becomes possible. Trajectory planning and coordination for connected and automated vehicles (CAVs) have been studied at isolated "signal-free" intersections and in "signal-free" corridors under the fully CAV environment in the literature. Most existing studies are based on the definition of approaching and exit lanes. The route a vehicle takes to pass through an intersection is determined by its movement. That is, only the origin and destination arms are included. This study proposes a mixed-integer linear programming (MILP) model to optimize vehicle trajectories at an isolated "signal-free" intersection without lane allocation, denoted as "lane-allocation-free" (LAF) control. Each lane can be used as both approaching and exit lanes for all vehicle movements including left-turn, through, and right-turn. A vehicle can take a flexible route by way of multiple arms to pass through the intersection. In this way, the spatial–temporal resources are expected to be fully utilized. The interactions between vehicle trajectories are modeled explicitly at the microscopic level. Vehicle routes and trajectories (i.e., car-following and lane-changing behaviors) at the intersection are optimized in one unified framework for system optimality in terms of total vehicle delay. Considering varying traffic conditions, the planning horizon is adaptively adjusted in the implementation of the proposed model to make a balance between solution feasibility and computational burden. Numerical studies validate the advantages of the LAF control in terms of both vehicle delay and throughput with different demand structures and temporal safety gaps.

1. Introduction

Internet of vehicles is an important part of internet of things, which enables the communication between vehicles (V2V) and between vehicles and infrastructure (V2I). Traffic information (e.g., signal timings, route guidance, and speed advisory) can be conveyed from intersections to vehicles for trajectory planning. At the same time, detailed vehicle trajectory data (e.g., locations and speeds) can be collected from vehicles for traffic management at intersections. Further, with the advances in automated driving technologies, connected and automated vehicles (CAVs) have caught the attention of the traffic community. The observability and controllability of CAVs lead to the revolution of traffic control from the traditional flow-based methods (e.g., signal control) to individual-based methods (e.g., trajectory control) (Li et al., 2014b; Pei et al., 2019), which have greater potential to improve the

* Corresponding authors.
E-mail addresses: haoruochen@tongji.edu.cn (R. Hao), zhyx@tongji.edu.cn (Y. Zhang), mawanjing@tongji.edu.cn (W. Ma), hughyu90@tongji.edu.cn (C. Yu), suntuo@tongji.edu.cn (T. Sun), b.vanarem@tudelft.nl (B. van Arem).

https://doi.org/10.1016/j.trc.2023.104152
Received 1 April 2022; Received in revised form 20 April 2023; Accepted 23 April 2023
Available online 10 May 2023

operational efficiency of traffic systems. With increasing traffic demand, vehicles suffer from severe traffic congestion, which causes environmental problems and economic losses (Koonce et al., 2008). Intersections are usually regarded as the bottlenecks for traffic flows in an urban road network. Traffic management at intersections is crucial to ensuring traffic efficiency, safety, energy economics, and pollution reduction. Traditionally, flow-based control methods such as priority rules (e.g., stop signs, roundabouts, right-before-left, etc.) and traffic signals are used to assign rights of way (ROW) to conflicting traffic flows at an intersection. Fixed-time control, vehicle-actuated control, and adaptive control are widely used in practice in terms of traffic signal control (Papageorgiou et al., 2003). Numerous studies have been dedicated to these research areas (Allsop, 1976; Webster, 1958; Little et al., 1981; Heydecker, 1992; Han et al., 2014; Han and Gayah, 2015; Liu and Smith, 2015; Memoli et al., 2017; Mohebifard and Hajbabaie, 2019; Mohajerpoor et al., 2019). However, individual-based traffic control remains to be investigated, which is currently a hot topic.

A thorough review on urban traffic signal control with CAVs was provided in Guo et al. (2019a). Generally, related studies fall into three categories. In the first category, real-time vehicle trajectory information (e.g., speeds and locations) is utilized for signal optimization with or without infrastructure-based detector data (e.g., traffic volumes from loop detectors) by catching time-varying traffic demand (Gradinescu et al., 2007; Feng et al., 2018a). Signal timings such as cycle lengths and green splits are optimized at isolated intersections (Gradinescu et al., 2007; Guler et al., 2014; Feng et al., 2015; Liang et al., 2018; Yang et al., 2017) and multiple intersections (He et al., 2012; Yang et al., 2017). The studies in the second category focus on vehicle trajectory planning on the basis of traffic information from intersections. One typical application is eco-driving, which optimizes vehicle trajectories with the objectives of minimizing fuel/energy consumption and emission. Typically, optimal control models or feedback control models are formulated with vehicle speeds or acceleration rates as the control variables (Kamal et al., 2013; Wang et al., 2014a,b; Ubiergo and Jin, 2016; Wan et al., 2016). Platooning can also be considered (Liu et al., 2019; Feng et al., 2019). Approximation has then been proposed to solve the models more efficiently by either discretizing time or segmenting trajectories (Wan et al., 2016; Kamalanathsharma and Rakha, 2013). In the third category, signal optimization and vehicle trajectory planning are integrated into one unified framework. However, limited studies have been reported. Li et al. (2014a) enumerated feasible signal plans and segmented vehicle trajectories for joint optimization. Feng et al. (2018b) proposed a dynamic programming model for signal optimization combined with an optimal control model for trajectory planning as a two-stage model. Yu et al. (2018) proposed a mixed-integer linear programming (MILP) model to simultaneously optimize signal timings and vehicle trajectories. Guo et al. (2019b) proposed a DP-SH (dynamic programming with shooting heuristic) algorithm for efficiency and jointly optimized vehicle trajectories and signal timings.

Assuming the fully CAV environment, the concept of “signal-free” intersections has been proposed (Dresner and Stone, 2004, 2008). Vehicles cooperate with each other and pass through intersections without physical traffic signals. One prevailing category of such studies are based on the philosophy of reservation. Approaching vehicles send requests to the intersection controller to reserve space and time slots within the intersection area. Reservation requests are managed to determine the service sequence of the approaching vehicles, usually according to rule-based policies such as “first-come, first-served” (FCFS) strategy (Au and Stone, 2010; Dresner and Stone, 2004, 2008; Li et al., 2013), priority strategy (Alonso et al., 2011), auction strategy (Carlino et al., 2013), and platooning strategy (Tachet et al., 2016). However, both theoretical analysis (Yu et al., 2019b) and numerical case studies (Levin et al., 2016) showed that the advantages of reservation-based control might not outperform conventional signal control (e.g., vehicle-actuated control) in certain cases. Because the optimality cannot be guaranteed due to the rule-based nature of reservation-based control. As a result, optimization-based models have been proposed. Typically, constrained nonlinear optimization models are formulated (Joyoung Lee, 2012; Zohdy and Rakha, 2016). In Joyoung Lee (2012), vehicle acceleration/deceleration rates were optimized to minimize trajectory overlap with the focus on safety. In Zohdy and Rakha (2016), vehicle arrival times at an intersection were optimized to minimize vehicle delay with the focus on efficiency. Qian et al. (2019) also optimized the vehicle arrival times but with a linear programming method. In addition, 3D CAV trajectories were mathematically formulated in the combined temporal-spatial domains (Li et al., 2019). Priority-based and Discrete Forward-Rolling Optimal Control (DFROC) algorithms were developed for CAV management at isolated intersections. Distributed control methods have also been investigated to alleviate computational burden (Mirheli et al., 2019), which have been successfully applied to the coordination and control of automated ground vehicles, automated underwater vehicles, and automated air vehicles (Keviczky et al., 2007; Kuwata and How, 2010; Makarem and Gillet, 2012; Campos et al., 2014; Zhang et al., 2016; Malikopoulos et al., 2018). Xu et al. (2018) projected approaching vehicles from different traffic movements into a virtual lane and then introduced a conflict-free geometry topology with the consideration of the conflict relationship of involved vehicles. Mirheli et al. (2019) proposed a vehicle-level mixed-integer non-linear programming model for cooperative trajectory planning in a distributed way. Vehicle-level solutions were pushed toward global optimality. However, in most of the distributed control methods, vehicles make decisions based on local traffic information and the system optimum cannot be guaranteed. Intersections may even be blocked due to the lack of vehicle cooperation from a systematic point of view (Li et al., 2019; Shahidi et al., 2011). The concept of safety buffers has been proposed to improve safety and efficiency under uncertain traffic environments (Dresner and Stone, 2008; Khayatian et al., 2018; Li et al., 2020; Aoki and Rajkumar, 2022; Lu et al., 2022).

Notwithstanding the abundant studies, it is noted that most of the studies do not take into consideration the interactions of vehicle trajectories at the microscopic level, which, however, is crucial to vehicle trajectory planning. Car-following behaviors are usually explicitly modeled while lane-changing behaviors are not. Recently, Yu et al. (2019a) successfully addressed this issue. Both car-following and lane-changing behaviors of vehicles in a “signal-free” corridor were cooperatively optimized in one unified framework. Approaching lanes were not specified with lane allocation, which is called “approaching-lane-allocation-free” (ALAF) in this paper. Each approaching lane could be used by all vehicle movements (i.e., left-turn, through, and right-turn). This study takes a further step and eliminates the definition of approaching and exit lanes. Similar concepts have been studied and the benefits

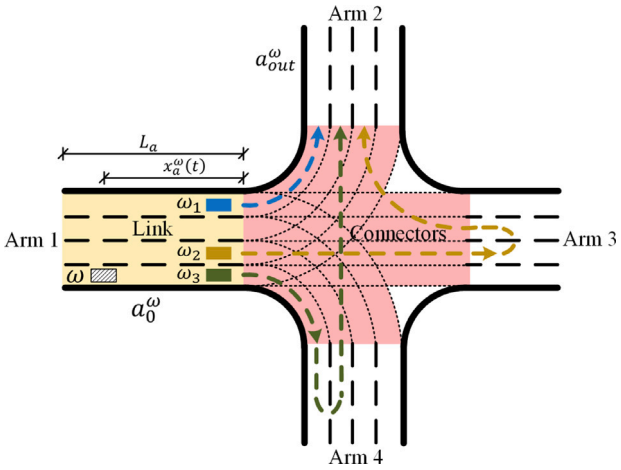

Fig. 1. A "signal-free" and "lane-allocation-free" intersection with four arms.

have been validated in Mitrovic et al. (2020) and Sun et al. (2017). But they focus on vehicle management in a link between two intersections where lane allocation of approaching and exit lanes is fixed. In contrast, there is no lane allocation in links or at intersections in this study. Each lane can be used by both approaching and leaving vehicles in all directions. Further, the route a vehicle takes to pass through the intersection is fixed in Yu et al. (2019a), which only consists of the origin and the destination arms.

In this study, a vehicle can take a flexible route by way of multiple arms. In this way, the spatial–temporal resources at intersections are expected to be fully utilized, especially with imbalanced traffic. To this end, this study proposes an MILP model to optimize vehicle routes and trajectories (i.e., car-following behaviors and lane-changing behaviors) at an isolated "signal-free" and "lane-allocation-free" intersection, which is denoted as "lane-allocation-free" (LAF) control. The centralized control is preferred to the decentralized control from the perspective of reducing vehicle delay and improving intersection capacity (Li et al., 2019). Although the centralized control is applied, V2V communication can be used and combined with V2I communication to collect vehicle states for the centralized controller and send trajectory strategies from the controller to vehicles (Dikaiakos et al., 2007). To balance solution feasibility and computational burden, the planning horizon is adaptively adjusted in the implementation procedure with varying traffic conditions.

The remainder of this paper is organized as follows. Section 2 describes the problem and presents the notations. Section 3 formulates the MILP model to optimize vehicle routes and trajectories at a "signal-free" and "lane-allocation-free" intersection. Section 4 presents the implementation procedure of the proposed model with varying traffic conditions, which adaptively adjusts the planning horizon to improve computational efficiency. Numerical studies are conducted in Section 5. Finally, conclusions and recommendations are provided in Section 6.

2. Problem description and notations

2.1. Problem description

Fig. 1 shows a "signal-free" and "lane-allocation-free" intersection with four arms as an example. In this study, one arm consists of an undirected link and all directed connectors departing from the link. For example, arm 1 has four connectors for left-turn traffic, four for through traffic, and four for right-turn traffic. Fig. 1 highlights the link part and the connector part of arm 1. In contrast with conventional intersections, no approaching lanes or exit lanes are defined, and no lane allocation is specified. That is, each lane can be used by both approaching and leaving vehicles in all directions in the control zone at the intersection. Note that the control zone should be covered by the communication range of the intersection controller.

Conventionally, the route of a vehicle is fixed at an intersection. For example, vehicle ω in arm 1 tries to turn left in Fig. 1. It follows the trajectory of vehicle ω_1 under conventional traffic management. That is, the route of vehicle ω only consists of arm 1 and arm 2. If vehicle ω conflicts with other vehicles, it may wait at the stop line location, blocking the traffic behind. Suppose there is heavy through traffic, light left-turn traffic in arm 1 and light traffic in arm 4. Left-turn vehicle ω is waiting in the rightmost lane in arm 1, looking for the gaps between the through vehicles in the remaining three lanes. As a result, only three lanes in arm 1 can be fully utilized at the same time. To improve the efficiency of the intersection system, flexible routing is considered in this study. Flexible routing means that vehicle ω can travel to other arms before entering the destination arm 2, e.g., following the trajectory of vehicle ω_3. In this way, vehicle ω can wait in arm 4 instead of arm 1, and the four lanes in arm 1 can be fully utilized by the heavy through traffic. The trajectory of vehicle ω_2 is another possible route. In this way, it is expected the spatial–temporal resources can be better utilized at the intersection.

Given the geometric layout of the intersection and the vehicles in the control zone (L_a), the objective of this study is to cooperatively optimize the routes and the trajectories of the vehicles for minimizing total delay. The route plan of vehicle ω is the selection of arms to be visited between the origin arm a_0^ω, in which vehicle ω is traveling, and the destination arm a_{out}^ω as well as the arm sequence. The trajectory of vehicle ω is determined by the lane choice ($\delta_k^\omega(t)$) and the longitudinal location ($x_a^\omega(t)$) in each visited arm at each time step t. Note that a_0^ω is updated when vehicle ω enters a new arm. For example, a_0^ω is arm 1 in Fig. 1 and vehicle ω follows the trajectory of vehicle ω_3. a_0^ω becomes arm 4 when vehicle ω travels in arm 4. $\mathbf{A}^\omega$ is then introduced to store the arms that vehicle ω has not visited. In Fig. 1, $\mathbf{A}^\omega = \{\text{arm } 2, \text{arm } 3, \text{arm } 4\}$ when vehicle ω is in arm 1 and $\mathbf{A}^\omega = \{\text{arm } 2, \text{arm } 3\}$ when vehicle ω travels into arm 4.

To simplify the formulations, the following assumptions are made:

- All vehicles are CAVs and can be controlled by a centralized controller.
- The destination arm of a vehicle does not change after the vehicle enters the control zone.
- Vehicles follow the connectors and do not change lanes when traveling within the intersection area.
- Vehicles travel at constant speeds in connectors. The speed is determined by the radius of a connector.
- Vehicles can change lanes instantly in the link part of each arm.
- Vehicle motion is captured by the first order model, the same assumption as in Newell's car-following model (Newell, 2002).
- When there is congestion, vehicles may have to wait outside the control zone until the queueing vehicles in the control zone are discharged.

2.2. Notations

Main notations applied hereafter are summarized in this part. They will be explained in detail in the formulations (see Table 1).

3. Formulations

This section presents the MILP model based on discrete time to cooperatively optimize the routes and the trajectories of the vehicles in the control zone. The constraints and the objective function are presented in the following sub-sections.

3.1. Constraints

Decision variable related constraints, vehicle motion related constraints, and safety related constraints are introduced in this section. The decision variables are constrained by variable domains and boundary conditions at the start and end of the planning horizon. The vehicle motion constraints deal with route planning, vehicle longitudinal motion, and lane choices when entering or leaving the link part of an arm. The safety constraints guarantee spatial/temporal safety gaps between vehicles traveling in arms or within the intersection area.

3.1.1. Domains of decision variables

There are three main types of decision variables for each vehicle ω in each arm a, namely, the longitudinal location, the lane choice, and the entering and leaving time points. $x_a^\omega(t)$ is the distance between vehicle ω and the stop line location in arm a at time step t. $x_a^\omega(t)$ is positive when vehicle ω is in the link part of arm a. And $x_a^\omega(t)$ is negative when vehicle ω is in the connector part of arm a. $\delta_k^\omega(t)$ indicates the lane choice of vehicle ω. $\delta_k^\omega(t) = 1$ if vehicle ω is in lane k at time step t. $\underline{t}_a^\omega$ and $\bar{t}_a^\omega$ are the time points of entering and leaving the link part of arm a, respectively. $\bar{t}_a^\omega$ is the time of leaving the control zone if arm a is the destination arm a_{out}^ω. $\underline{t}_a^\omega$ and $\bar{t}_a^\omega$ are continuous and they are relative values to the current time t_0.

Denote a_0^ω as the origin arm, in which vehicle ω is traveling. If vehicle ω is in the link part of arm a_0^ω, then $\underline{t}_a^\omega$ and $\bar{t}_a^\omega$ are constrained by

$$\underline{t}_a^\omega = \underline{t}_0^\omega \le 0, \forall a = a_0^\omega; \omega \in \mathbf{\Omega} \tag{1}$$

$$0 \le \bar{t}_a^\omega \le T \cdot \Delta t, \forall a = a_0^\omega; \omega \in \mathbf{\Omega} \tag{2}$$

where $\underline{t}_0^\omega$ is the recorded time point of entering the link of arm a_0^ω, which is a relative value to the current time t_0; $\mathbf{\Omega}$ is the set of vehicles in the control zone. $\underline{t}_a^\omega$ is non-positive according to Eq. (1). If vehicle ω is in the connector part of arm a, then the following constraint of $\bar{t}_a^\omega$ is added instead of Eq. (2):

$$\bar{t}_a^\omega = \bar{t}_0^\omega \le 0, \forall a = a_0^\omega; \omega \in \mathbf{\Omega} \tag{3}$$

where $\bar{t}_0^\omega$ is the recorded time point of leaving the link of arm a, which is a relative value to the current time t_0.

For other arms (i.e., $a \neq a_0^\omega$), $\underline{t}_a^\omega$ and $\bar{t}_a^\omega$ are constrained by Eqs. (4)–(7):

$$0 \le \underline{t}_a^\omega \le T \cdot \Delta t + \mathrm{M}\left(1 - \beta_a^\omega\right), \forall a \in \mathbf{A}, a \neq a_0^\omega; \omega \in \mathbf{\Omega} \tag{4}$$

$$\underline{t}_a^\omega \le \bar{t}_a^\omega \le T \cdot \Delta t + \mathrm{M}\left(1 - \beta_a^\omega\right), \forall a \in \mathbf{A}, a \neq a_0^\omega; \omega \in \mathbf{\Omega} \tag{5}$$

Table 1
Notations.

General notations	
M:	A sufficiently large number
t:	Time step
$\mathbf{\Omega}$:	Set of vehicles in the control zone of the intersection; each vehicle is denoted as ω
$\mathbf{A}$:	Set of arms of the intersection; each arm is denoted as a
a_0^ω:	Origin arm in which vehicle ω is traveling when the optimization is conducted
a_{out}^ω:	Destination arm in which vehicle ω leaves the control zone of the intersection
$\mathbf{A}^\omega$:	Set of arms that vehicle ω has not visited; if vehicle ω is in arm a_{out}^ω, then $\mathbf{A}^\omega = \emptyset$
$\mathbf{A}_0^\omega$:	Set of arms that vehicle ω is visiting or has not visited; $\mathbf{A}_0^\omega = \mathbf{A}^\omega \cup \{a_0^\omega\}$
$\mathbf{K}_a$:	Set of lanes in arm a; each lane is denoted as k
k_a^{left}:	Leftmost lane of arm a facing the stop line
k_a^{right}:	Rightmost lane of arm a facing the stop line
k^{left}:	Left adjacent lane of lane k facing the stop line
k^{right}:	Right adjacent lane of lane k facing the stop line
$\mathbf{K}_{a_1}^{a_2}$:	Set of lanes in arm a_1 that are connected to the lanes in arm a_2
$\mathbf{K}_{out}^\omega$:	Set of lanes in the destination arm in which vehicle ω leaves the control zone
k_+^a:	Succeeding lane of lane k in arm a; that is, lane k_+^a is connected from lane k by a connector
$\langle k_1, k_2 \rangle$:	Connector from lane k_1 to lane k_2
$\mathbf{P}_{k_1,k_2}^{k_3,k_4}$:	Set of conflict points between connector $\langle k_1, k_2 \rangle$ and connector $\langle k_3, k_4 \rangle$; each conflict point is denoted as p
Parameters	
Δt:	Length of time step, s
t_0:	Current time when vehicle routes and trajectories are optimized, which indicates the start of the planning horizon (i.e., $t = 0$), s
T:	Planning horizon; the horizon duration is $T \cdot \Delta t$
T_0:	Initial value of T in the implementation procedure for adaptively adjusting T
ΔT:	Step length for adjusting T in the implementation procedure
T^{turn}:	Time steps of turning around; the turning around time is $T^{turn} \cdot \Delta t$
L_a:	Length of the link part of arm a in the control zone, m
V_a:	Speed limit in the link part of arm a, m/s
$l_{k_1}^{k_2}$:	Length of connector $\langle k_1, k_2 \rangle$ that connects lane k_1 and lane k_2, m
l_{k_1,k_2}^p:	Distance between the start of connector $\langle k_1, k_2 \rangle$ and conflict point p, m
$v_{k_1}^{k_2}$:	Travel speed in connector $\langle k_1, k_2 \rangle$, m/s
τ:	Temporal safety gap, s
d :	Spatial safety gap, m
$\tilde{x}^\omega$:	Distance between vehicle ω and the stop line location in the current arm at the current time step, m
$\tilde{\delta}_k^\omega$:	1, if vehicle ω is in lane k in the current arm at the current time step; 0, otherwise
$\tilde{dir}_a^\omega$:	1, if vehicle ω is driving toward the stop line at the current time step; 0, otherwise
$\tilde{\gamma}_{a_1,a_2}^\omega$:	1, if vehicle ω plans to travel from arm a_1 to arm a_2 according the previous optimization; 0, otherwise
$\underline{t}_0^\omega$:	Recorded time point when vehicle ω entered the link part of the current arm, which is a relative value to the current time, s
$\bar{t}_0^\omega$:	Recorded time point when vehicle ω left the link part of the current arm into a connector, which is a relative value to the current time, s
w_1/w_2:	Weighting parameter in the objective function
Decision variables	
$x_a^\omega(t)$:	Distance from vehicle ω to the stop line location in arm a at time step t, m
$\delta_k^\omega(t)$:	1, if vehicle ω is in lane k at time step t; 0, otherwise
$\underline{t}_a^\omega / \bar{t}_a^\omega$:	Time point of entering/leaving the link part of arm a for vehicle ω, s
$\bar{t}_{a_{out}^\omega}^\omega$:	the time when vehicle ω leaves the link part of the destination arm a_{out}^ω
γ_{a_1,a_2}^ω:	1, if vehicle ω plans to travel from arm a_1 to arm a_2 in the following time; 0, otherwise
Auxiliary variables	
$\underline{\mu}_a^\omega(t)$:	1, if $t \cdot \Delta t \geq \underline{t}_a^\omega$; 0, otherwise
$\bar{\mu}_a^\omega(t)$:	1, if $t \cdot \Delta t \geq \bar{t}_a^\omega$; 0, otherwise
$dir_a^\omega(t)$:	1, if vehicle ω drives toward the stop line of arm a; 0, otherwise
$ta_a^\omega(t)$:	1, if vehicle ω turns around in arm a at time step t; 0, otherwise
$tal_a^\omega(t)$:	1, if vehicle ω turns around by using the left adjacent lane in arm a at time step t; 0, otherwise
$tar_a^\omega(t)$:	1, if vehicle ω turns around by using the right adjacent lane in arm a at time step t; 0, otherwise
β_a^ω:	1, if vehicle ω plans to visit arm a in the following time; 0, otherwise
v_a^ω:	Travel speed within the intersection area after vehicle ω leaves arm a, m/s
$\pi_{k_1,k_2}^{\omega_1,\omega_2}$:	0, if vehicle ω_1 enters connector $\langle k_1, k_2 \rangle$ after vehicle ω_2 leaves connector $\langle k_2, k_1 \rangle$; 1, otherwise
$\rho_a^{\omega_1,\omega_2}(t)$	1, if vehicle ω_1 and vehicle ω_2 travel in the same lane in the link part of arm a at time step t; $\rho_a^{\omega_1,\omega_2}(t)$ can be one or zero, otherwise

$$-\mathrm{M}\beta_a^\omega \leq \underline{t}_a^\omega - 2T \cdot \Delta t \leq \mathrm{M}\beta_a^\omega, \forall a \in \mathbf{A}, a \neq a_0^\omega; \omega \in \mathbf{\Omega} \tag{6}$$

$$-\mathrm{M}\beta_a^\omega \leq \bar{t}_a^\omega - 2T \cdot \Delta t \leq \mathrm{M}\beta_a^\omega, \forall a \in \mathbf{A}, a \neq a_0^\omega; \omega \in \mathbf{\Omega} \tag{7}$$

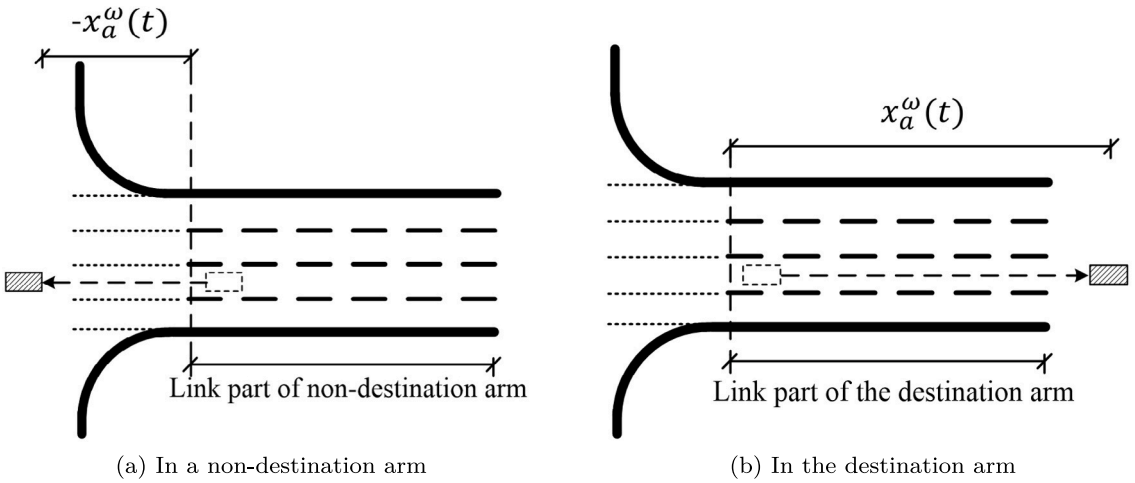

(a) In a non-destination arm (b) In the destination arm

Fig. 2. Illustration of a vehicle leaving a link part.

where $\beta_a^\omega = 1$ if arm a is on the planned route of vehicle ω and $\beta_a^\omega = 0$, otherwise. If vehicle ω plans to visit arm a (i.e., $\beta_a^\omega = 1$), then Eqs. (4) and (5) are effective. Otherwise, Eqs. (6) and (7) are effective. In that case, $\underline{t}_a^\omega$ and $\bar{t}_a^\omega$ are set as $2T \cdot \Delta t$, which means that vehicle ω will never enter arm a in the planning horizon.

Before vehicle ω enters the link part of arm a, $x_a^\omega(t)$ is defined as zero:

$$-\mathrm{M}\underline{\mu}_a^\omega(t) \le x_a^\omega(t) \le \mathrm{M}\underline{\mu}_a^\omega(t), \forall t = 0, \dots, T; a \in \mathbf{A}; \omega \in \mathbf{\Omega} \tag{8}$$

where $\underline{\mu}_a^\omega(t)$ is an auxiliary binary variable. $\underline{\mu}_a^\omega(t) = 1$ if vehicle ω has entered arm a by time step t; $\underline{\mu}_a^\omega(t) = 0$, otherwise. Eq. (8) guarantees that $x_a^\omega(t) = 0$ when $\underline{\mu}_a^\omega(t) = 0$.

When vehicle ω travels in the link part of arm a, $x_a^\omega(t)$ is bounded by

$$-\mathrm{M}\left(1 - \underline{\mu}_a^\omega(t) + \bar{\mu}_a^\omega(t)\right) \le x_a^\omega(t) \le L_a, \forall t = 0, \dots, T; a \in \mathbf{A}; \omega \in \mathbf{\Omega} \tag{9}$$

where L_a is the length of arm a within the control zone; $\bar{\mu}_a^\omega(t)$ is an auxiliary binary variable. $\bar{\mu}_a^\omega(t) = 1$ if vehicle ω has left the link part of arm a by time step t; $\bar{\mu}_a^\omega(t) = 0$, otherwise. $\mathbf{A}_0^\omega$ is the set of arms that vehicle ω is visiting or has not visited, which is updated when vehicle ω enters an arm. Eq. (9) guarantees that $0 \le x_a^\omega(t) \le L_a$ when $\underline{\mu}_a^\omega(t) = 1$ and $\bar{\mu}_a^\omega(t) = 0$.

After vehicle ω leaves the link part of arm $a \ne a_{out}^\omega$ (i.e., $\bar{\mu}_a^\omega(t) = 1$), $x_a^\omega(t)$ is defined as a negative value, as shown in Fig. 2(a):

$$\begin{aligned} &-\mathrm{M}\left(1 - \bar{\mu}_a^\omega(t)\right) \le x_a^\omega(t) + v_a^\omega\left(t \cdot \Delta t - \bar{t}_a^\omega\right) \le \mathrm{M}\left(1 - \bar{\mu}_a^\omega(t)\right) \\ &\forall t = 0, \dots, T; a \in \mathbf{A}_0^\omega, a \ne a_{out}^\omega; \omega \in \mathbf{\Omega} \end{aligned} \tag{10}$$

where v_a^ω is the travel speed of vehicle ω in the connector part of arm a; $t \cdot \Delta t - \bar{t}_a^\omega$ is the travel time in the connector part at time step t. Eq. (10) indicates that $x_a^\omega(t) = -v_a^\omega\left(t \cdot \Delta t - \bar{t}_a^\omega\right)$ when $\bar{\mu}_a^\omega(t) = 1$. v_a^ω is determined by the planned route and the lane choice of vehicle ω when leaving the link part of arm a:

$$\begin{aligned} &-\mathrm{M}\left(2 - \gamma_{a_1,a_2}^\omega - \delta_{k_1}^\omega(T)\right) \le v_{a_1}^\omega - v_{k_1}^{k_2} \le \mathrm{M}\left(2 - \gamma_{a_1,a_2}^\omega - \delta_{k_1}^\omega(T)\right) \\ &\forall k_2 = k_{1+}^{a_2}; k_1 \in \mathbf{K}_{a_1}^{a_2}; a_2 \in \mathbf{A}^\omega, a_2 \ne a_1; a_1 \in \mathbf{A}_0^\omega, a_1 \ne a_{out}^\omega; \omega \in \mathbf{\Omega} \end{aligned} \tag{11}$$

where $\mathbf{A}^\omega$ is the set of arms that have not been visited, which is updated when vehicle ω enters an arm; $\mathbf{K}_{a_1}^{a_2}$ is the set of lanes in arm a_1 that are connected to the lanes in arm a_2; $k_{1+}^{a_2}$ is the lane in arm a_2 that is connected from lane k_1 in arm a_1; $v_{k_1}^{k_2}$ is the travel speed in connector $\langle k_1, k_2 \rangle$. If vehicle ω travels from lane k_1 in arm a_1 to lane k_2 in arm a_2 (i.e., $\gamma_{a_1,a_2}^\omega = \delta_{k_1}^\omega(T) = 1$), Eq. (11) sets $v_{a_1}^\omega = v_{k_1}^{k_2}$. Note that the final time step T is used in Eq. (11) because $\delta_k^\omega(t)$ will be constrained to remain the same after vehicle ω leaves the link part of an arm in the following constraints.

After vehicle ω leaves the destination arm $a = a_{out}^\omega$ (i.e., $\bar{\mu}_a^\omega(t) = 1$), $x_a^\omega(t)$ is set as $L_a + V_a\left(t \cdot \Delta t - \bar{t}_a^\omega\right)$ as shown in Fig. 2:

$$\begin{aligned} &-\mathrm{M}\left(1 - \bar{\mu}_a^\omega(t)\right) \le x_a^\omega(t) - \left(L_a + V_a\left(t \cdot \Delta t - \bar{t}_a^\omega\right)\right) \le \mathrm{M}\left(1 - \bar{\mu}_a^\omega(t)\right) \\ &\forall t = 0, \dots, T; a = a_{out}^\omega; \omega \in \mathbf{\Omega} \end{aligned} \tag{12}$$

where V_a is the speed limit in arm a; $t \cdot \Delta t - \bar{t}_a^\omega$ is the travel time in arm a outside the control zone.

3.1.2. Boundary conditions

Boundary condition constraints deal with the states (the longitudinal location, the lane choice, and the driving direction) of vehicles at the beginning and the end of the planning horizon. For the origin arm $a = a_0^\omega$ of vehicle ω, $x_a^\omega(0)$ is determined by the

current location of vehicle ω:

$$x_a^\omega(0) = \tilde{x}^\omega, \forall a = a_0^\omega; \omega \in \mathbf{\Omega} \tag{13}$$

where $\tilde{x}^\omega$ is the distance between vehicle ω and the stop line location in the origin arm a_0^ω at the current time. Similarly, the lane choice $\delta_k^\omega(0)$ in the origin arm $a = a_0^\omega$ is determined as well:

$$\delta_k^\omega(0) = \tilde{\delta}_k^\omega, \forall k \in \mathbf{K}_a; a = a_0^\omega; \omega \in \mathbf{\Omega} \tag{14}$$

where $\mathbf{K}_a$ is the set of lanes in arm a. $\tilde{\delta}_k^\omega = 1$ if vehicle ω is in lane k at the current time; $\tilde{\delta}_k^\omega = 0$, otherwise. Apart from the initial lane and location, the initial driving direction is also determined:

$$dir_a^\omega(0) = \tilde{dir}_a^\omega, \forall a = a_0^\omega; \omega \in \mathbf{\Omega} \tag{15}$$

where $\tilde{dir}_a^\omega$ is the driving direction of vehicle ω in the origin arm a_0^ω at the current time. The driving directions in other arms are initialized as

$$dir_a^\omega(0) = 1, \forall a \neq a_0^\omega; \omega \in \mathbf{\Omega} \tag{16}$$

At the end of the planning horizon, each vehicle ω is supposed to have left the control zone of the intersection:

$$x_a^\omega(T) > L_a, \forall a = a_{out}^\omega; \omega \in \mathbf{\Omega} \tag{17}$$

3.1.3. Route planning

Due to the flexible routing, vehicles can traverse a sequence of arms before leaving the intersection. The route planning constraints deal with the selection of arms to traverse as well as the sequence. Denote γ_{a_1,a_2}^ω as the indicator of the arm sequence on the route of vehicle ω. $\gamma_{a_1,a_2}^\omega = 1$ if vehicle ω plans to travel from arm a_1 to arm a_2; $\gamma_{a_1,a_2}^\omega = 0$, otherwise. For the convenience of modeling, γ_{a_1,a_2}^ω is set as zero if $a_1 = a_2$:

$$\gamma_{a,a}^\omega = 0, \forall a \in \mathbf{A}; \omega \in \mathbf{\Omega} \tag{18}$$

Each arm can be visited at most once by each vehicle, which is specified by Eqs. (19) and (20):

$$\sum_{a_1 \in \mathbf{A}} \gamma_{a_1,a_2}^\omega \leq 1, \forall a_2 \in \mathbf{A}; \omega \in \mathbf{\Omega} \tag{19}$$

$$\sum_{a_2 \in \mathbf{A}} \gamma_{a_1,a_2}^\omega \leq 1, \forall a_1 \in \mathbf{A}; \omega \in \mathbf{\Omega} \tag{20}$$

where $\sum_{a_1 \in \mathbf{A}} \gamma_{a_1,a_2}^\omega$ is the number of entering arm a_2; $\sum_{a_2 \in \mathbf{A}} \gamma_{a_1,a_2}^\omega$ is the number of leaving arm a_1.

If vehicle ω has visited arm a (i.e., $a \in \mathbf{A} \setminus \mathbf{A}_0^\omega$), then it will not visit this arm in the following time, which is specified by Eqs. (21) and (22):

$$\sum_{a_1 \in \mathbf{A}} \gamma_{a_1,a_2}^\omega = 0, \forall a_2 \in \mathbf{A} \setminus \mathbf{A}_0^\omega; \omega \in \mathbf{\Omega} \tag{21}$$

$$\sum_{a_2 \in \mathbf{A}} \gamma_{a_1,a_2}^\omega = 0, \forall a_1 \in \mathbf{A} \setminus \mathbf{A}_0^\omega; \omega \in \mathbf{\Omega} \tag{22}$$

Generally, there may be no connectors connecting arm a_1 and arm a_2, e.g., because of forbidden vehicle movements. In that case, $\mathbf{K}_{a_1}^{a_2}$ is an empty set. Then, γ_{a_1,a_2}^ω should be zero if $\mathbf{K}_{a_1}^{a_2}$ is empty:

$$\gamma_{a_1,a_2}^\omega \leq \left|\mathbf{K}_{a_1}^{a_2}\right|, \forall a_1, a_2 \in \mathbf{A}, a_1 \neq a_2; \omega \in \mathbf{\Omega} \tag{23}$$

where $\left|\mathbf{K}_{a_1}^{a_2}\right|$ is the size of $\mathbf{K}_{a_1}^{a_2}$ (i.e., the number of the elements in $\mathbf{K}_{a_1}^{a_2}$).

If the origin arm a_0^ω is not the destination arm a_{out}^ω (i.e., $a_0^\omega \neq a_{out}^\omega$), then vehicle ω will not enter arm a_0^ω from other arms in the following time but leave arm a_0^ω to other arms:

$$\sum_{a_1 \in \mathbf{A}} \gamma_{a_1,a_2}^\omega = 0, \forall a_2 = a_0^\omega, a_2 \neq a_{out}^\omega; \omega \in \mathbf{\Omega} \tag{24}$$

$$\sum_{a_2 \in \mathbf{A}} \gamma_{a_1,a_2}^\omega = 1, \forall a_1 = a_0^\omega, a_1 \neq a_{out}^\omega; \omega \in \mathbf{\Omega} \tag{25}$$

If a non-destination arm a_1 is to be visited by vehicle ω (i.e., $a_1 \in \mathbf{A}^\omega, a_1 \neq a_{out}^\omega$), then the number of entering arm a_1 should be equal to the number of leaving arm a_1, which are both one or zero:

$$\sum_{a_2 \in \mathbf{A}} \gamma_{a_1,a_2}^\omega = \sum_{a_2 \in \mathbf{A}} \gamma_{a_2,a_1}^\omega, \forall a_1 \in \mathbf{A}^\omega, a_1 \neq a_{out}^\omega; \omega \in \mathbf{\Omega} \tag{26}$$

If the destination arm a_{out}^{ω} is not the origin one (i.e., $a_{out}^{\omega} \neq a_0^{\omega}$), then vehicle ω will enter arm a_{out}^{ω} to leave the intersection from other arms in the following planning horizon:

$$\sum_{a_1 \in \mathbf{A}} \gamma_{a_1,a_2}^{\omega} = 1, \forall a_2 = a_{out}^{\omega}, a_2 \neq a_0^{\omega}; \omega \in \mathbf{\Omega} \tag{27}$$

$$\sum_{a_2 \in \mathbf{A}} \gamma_{a_1,a_2}^{\omega} = 0, \forall a_1 = a_{out}^{\omega}, a_1 \neq a_0^{\omega}; \omega \in \mathbf{\Omega} \tag{28}$$

If the destination arm a_{out}^{ω} is the origin one (i.e., $a_{out}^{\omega} = a_0^{\omega}$), then vehicle ω will not travel from other arms to arm a_{out}^{ω} or from arm a_{out}^{ω} to other arms. It only travels in the destination arm until it leaves the control zone.

$$\sum_{a_1 \in \mathbf{A}} \gamma_{a_1,a_2}^{\omega} = \sum_{a_1 \in \mathbf{A}} \gamma_{a_2,a_1}^{\omega} = 0, \forall a_2 = a_{out}^{\omega}, a_2 = a_0^{\omega}; \omega \in \mathbf{\Omega} \tag{29}$$

If vehicle ω is traveling in the connector part of the origin arm a_0^{ω}, then vehicle ω does not change lanes within the intersection area. That is, the succeeding arm remains the same:

$$\gamma_{a_1,a_2}^{\omega} = \tilde{\gamma}_{a_1,a_2}^{\omega}, \forall a_2 \in \mathbf{A}; a_1 = a_0^{\omega}; \omega \in \mathbf{\Omega} \tag{30}$$

where $\tilde{\gamma}_{a_1,a_2}^{\omega}$ indicates the route planned in the previous optimization.

$\beta_{a_1}^{\omega}$ is introduced to indicate whether vehicle ω plans to visit arm a_1 in the following time. If so, $\beta_{a_1}^{\omega} = 1$; otherwise, $\beta_{a_1}^{\omega} = 0$. This is guaranteed by

$$-\left(\sum_{a_2 \in \mathbf{A}} \gamma_{a_1,a_2}^{\omega} + \sum_{a_2 \in \mathbf{A}} \gamma_{a_2,a_1}^{\omega}\right) \leq \beta_{a_1}^{\omega} \leq \sum_{a_2 \in \mathbf{A}} \gamma_{a_1,a_2}^{\omega} + \sum_{a_2 \in \mathbf{A}} \gamma_{a_2,a_1}^{\omega}, \forall a_1 \in \mathbf{A}; \omega \in \mathbf{\Omega} \tag{31}$$

$$\sum_{a_2 \in \mathbf{A}} \gamma_{a_1,a_2}^{\omega} \leq \beta_{a_1}^{\omega}, \forall a_1 \in \mathbf{A}; \omega \in \mathbf{\Omega} \tag{32}$$

$$\sum_{a_1 \in \mathbf{A}} \gamma_{a_1,a_2}^{\omega} \leq \beta_{a_2}^{\omega}, \forall a_2 \in \mathbf{A}; \omega \in \mathbf{\Omega} \tag{33}$$

If vehicle ω does not plan to visit arm a_1 (i.e., $\sum_{a_2 \in \mathbf{A}} \gamma_{a_1,a_2}^{\omega} = \sum_{a_2 \in \mathbf{A}} \gamma_{a_2,a_1}^{\omega} = 0$), then Eq. (31) guarantees that $\beta_{a_1}^{\omega} = 0$. Otherwise, Eqs. (32) and (33) guarantee that $\beta_{a_1}^{\omega} = 1$. Eqs. (32) and (33) are both set in case of the origin arm and the destination arm. Because vehicle ω neither travels from other arms into the origin arm nor travels from the destination arm to other arms.

3.1.4. Vehicle longitudinal motions

The constraints of vehicle longitudinal motions deal with the longitudinal location, the driving direction, and the turning round maneuver in each arm. If vehicle ω enters the link part of an arm during time step $t+1$ (i.e., $\underline{\mu}_a^{\omega}(t) = 0$ and $\underline{\mu}_a^{\omega}(t+1) = 1$) as shown in Fig. 3(a), the traveled distance in the link part during this time step is constrained by the speed limit V_a in arm a:

$$\begin{aligned} &x_a^{\omega}(t+1) \leq V_a\left((t+1)\Delta t - \underline{t}_a^{\omega}\right) + \mathrm{M}\left(1 + \underline{\mu}_a^{\omega}(t) - \underline{\mu}_a^{\omega}(t+1)\right) \\ &\forall t = 0, \ldots, T-1; a \in \mathbf{A}_0^{\omega}; \omega \in \mathbf{\Omega} \end{aligned} \tag{34}$$

where $\underline{\mu}_a^{\omega}(t)$ is an auxiliary variable. $\underline{\mu}_a^{\omega}(t) = 1$ if vehicle ω has entered the link part of arm a by time step t; $\underline{\mu}_a^{\omega}(t) = 0$, otherwise. $(t+1)\Delta t - \underline{t}_a^{\omega}$ is the travel time in arm a within time step $t+1$.

If vehicle ω travels in the link part of an arm during time step $t+1$ (i.e., $\underline{\mu}_a^{\omega}(t) = 1$ and $\bar{\mu}_a^{\omega}(t+1) = 0$) as shown in Fig. 3(b), there are similar constraints:

$$\begin{aligned} &\left|x_a^{\omega}(t+1) - x_a^{\omega}(t)\right| \leq V_a \Delta t + \mathrm{M}\left(1 - \underline{\mu}_a^{\omega}(t) + \bar{\mu}_a^{\omega}(t+1)\right) \\ &\forall t = 0, \ldots, T-1; a \in \mathbf{A}_0^{\omega}; \omega \in \mathbf{\Omega} \end{aligned} \tag{35}$$

where $\bar{\mu}_a^{\omega}(t)$ is an auxiliary variable. $\bar{\mu}_a^{\omega}(t) = 1$ if vehicle ω has left the link part of arm a by time step t; $\bar{\mu}_a^{\omega}(t) = 0$, otherwise. Since vehicle ω can move both forward and backward, the absolute value function is used in Eq. (35).

If vehicle ω leaves the link part of a non-destination arm $a \neq a_{out}^{\omega}$ during time step $t+1$ (i.e., $\bar{\mu}_a^{\omega}(t) = 0$ and $\bar{\mu}_a^{\omega}(t+1) = 1$) as shown in Fig. 3(c), there are:

$$\begin{aligned} &x_a^{\omega}(t) \leq V_a\left(\bar{t}_a^{\omega} - t \cdot \Delta t\right) + \mathrm{M}\left(1 + \bar{\mu}_a^{\omega}(t) - \bar{\mu}_a^{\omega}(t+1)\right) \\ &\forall t = 0, \ldots, T-1; a \in \mathbf{A}_0^{\omega}, a \neq a_{out}^{\omega}; \omega \in \mathbf{\Omega} \end{aligned} \tag{36}$$

where $\bar{t}_a^{\omega} - t \cdot \Delta t$ is the travel time in the link part of arm a before vehicle ω leaves this link part within time step $t+1$.

If vehicle ω leaves the control zone in the destination arm a_{out}^{ω} during time step $t+1$ (i.e., $\bar{\mu}_a^{\omega}(t) = 0$ and $\bar{\mu}_a^{\omega}(t+1) = 1$) as shown in Fig. 3(d), there are:

$$\begin{aligned} &L_a - x_a^{\omega}(t) \leq V_a\left(\bar{t}_a^{\omega} - t \cdot \Delta t\right) + \mathrm{M}\left(1 + \bar{\mu}_a^{\omega}(t) - \bar{\mu}_a^{\omega}(t+1)\right) \\ &\forall t = 0, \ldots, T-1; a = a_{out}^{\omega}; \omega \in \mathbf{\Omega} \end{aligned} \tag{37}$$

different from Eq. (35), L_a is used in Eq. (37). Because vehicle ω leaves the control zone in the destination arm.

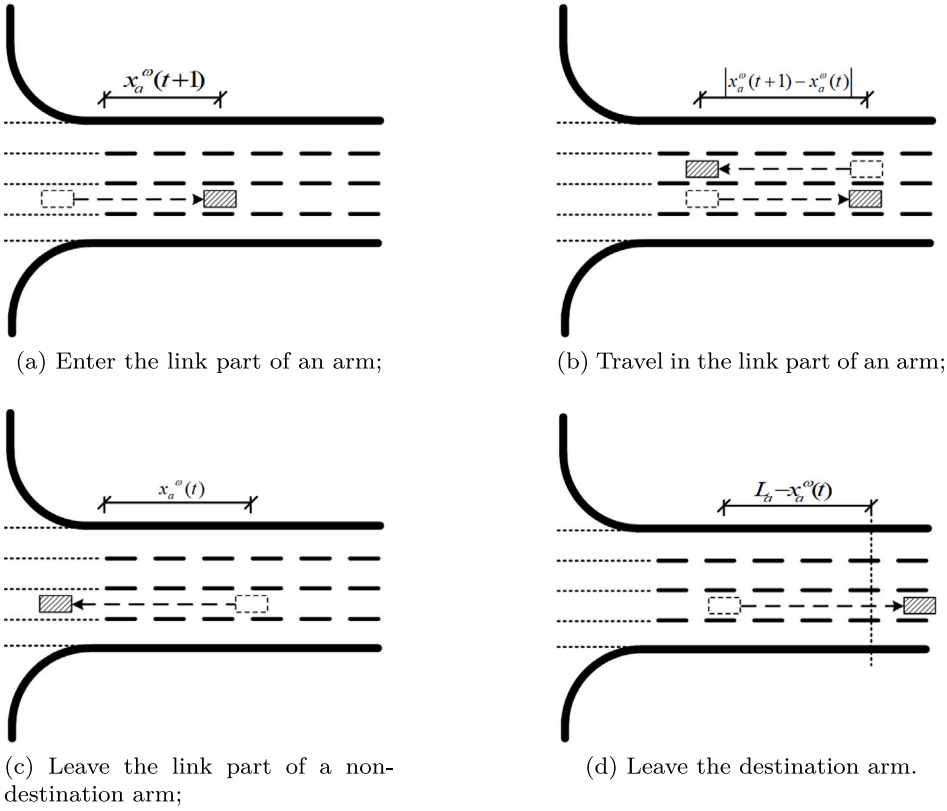

(a) Enter the link part of an arm; (b) Travel in the link part of an arm;

(c) Leave the link part of a non-destination arm; (d) Leave the destination arm.

Fig. 3. Illustration of vehicle movements.

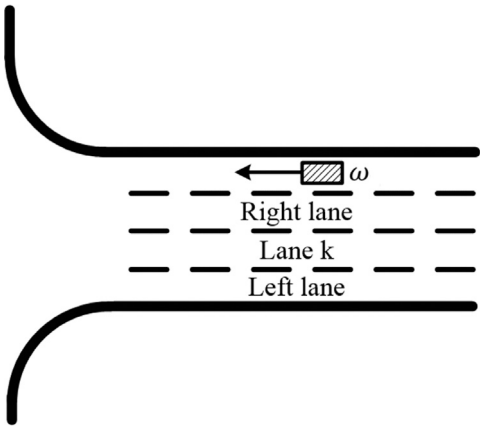

Fig. 4. Illustration of left and right adjacent lanes.

The relationship between the driving direction and the longitudinal location are constrained by Eqs. (38) and (39).

$$x_a^{\omega}(t+1) - x_a^{\omega}(t) \le \mathrm{M} dir_a^{\omega}(t), \forall t = 0, \ldots, T-1; \omega \in \mathbf{\Omega}; a \in \mathbf{A} \tag{38}$$

$$x_a^{\omega}(t) - x_a^{\omega}(t+1) \le \mathrm{M}\left(1 - dir_a^{\omega}(t)\right), \forall t = 0, \ldots, T-1; \omega \in \mathbf{\Omega}; a \in \mathbf{A} \tag{39}$$

where $dir_a^{\omega}(t)$ is the driving direction of vehicle ω in arm a at time step t. If $dir_a^{\omega}(t) = 0$, $x_a^{\omega}(t+1)$ will not be larger than $x_a^{\omega}(t)$, which means vehicles will always get close to the stop line, as shown in Fig. 4.

A vehicle will stay idling if it is turning around. This is guaranteed by Eq. (40).

$$\begin{aligned} &-\mathrm{M}\left(1-ta_a^{\omega}(t-t^{turn})\right) \le x_a^{\omega}(t)-x_a^{\omega}(t+1) \le \mathrm{M}\left(1-ta_a^{\omega}(t-t^{turn})\right) \\ &\forall t=0,\dots,T-1; t^{turn}=0,\dots,\min(t_0,T^{turn}); \omega\in\mathbf{\Omega}; a\in\mathbf{A} \end{aligned} \tag{40}$$

where $ta_a^{\omega}(t)$ is an auxiliary variable. $ta_a^{\omega}(t)=1$ if vehicle ω turns in arm a at time step t; $ta_a^{\omega}(t)=0$, otherwise. T^{turn} is the turning around time.

The driving direction has to change after turning around:

$$\begin{aligned} &1-\mathrm{M}\left(1-ta_a^{\omega}(t)\right) \le dir_a^{\omega}(t)+dir_a^{\omega}(t+1) \le 1+\mathrm{M}\left(1-ta_a^{\omega}(t)\right) \\ &\forall t=0,\dots,T-1; \omega\in\mathbf{\Omega}; a\in\mathbf{A} \end{aligned} \tag{41}$$

Eq. (41) indicates that $dir_a^{\omega}(t)+dir_a^{\omega}(t+1)=1$ if $ta_a^{\omega}(t)=1$. This means the driving directions of vehicle ω at time step t and time step $t+1$ will be different if vehicle ω turns around at time step t.

On the contrary, vehicles cannot change the driving direction without turning around:

$$\begin{aligned} &dir_a^{\omega}(t)-\mathrm{M}ta_a^{\omega}(t) \le dir_a^{\omega}(t+1) \le dir_a^{\omega}(t)+\mathrm{M}ta_a^{\omega}(t) \\ &\forall t=0,\dots,T-1; \omega\in\mathbf{\Omega}; a\in\mathbf{A} \end{aligned} \tag{42}$$

The turning-around maneuver takes T^{turn} time steps:

$$\begin{aligned} &-\left(1+ta_a^{\omega}(t-1)-ta_a^{\omega}(t)\right) \le ta_a^{\omega}(t+t^{turn}) \le 1+ta_a^{\omega}(t-1)-ta_a^{\omega}(t) \\ &\forall t=1,\dots,T-T^{turn}; t^{turn}=0,\dots,T^{turn}; \omega\in\mathbf{\Omega}; a\in\mathbf{A} \end{aligned} \tag{43}$$

If vehicle ω turns around at time step t (i.e., $ta_a^{\omega}(t-1)=0$ and $ta_a^{\omega}(t)=1$), then $ta_a^{\omega}(t)=0$ in the following T^{turn} time steps.

3.1.5. Lane choices

The constraints of lane choices deal with the lane-changing maneuvers with and without turning around. At any time step in the planning horizon, vehicle ω can only occupy one lane except when vehicle ω is turning around:

$$1+\sum_{t^{turn}=0}^{\min(t_0,T^{turn})} ta_a^{\omega}\left(t-t^{turn}\right)-(1-\beta_a^{\omega})\mathrm{M} \le \sum_{k\in\mathbf{K}_a}\delta_k^{\omega}(t) \le 1+\sum_{t^{turn}=0}^{\min(t_0,T^{turn})} ta_a^{\omega}\left(t-t^{turn}\right)+(1-\beta_a^{\omega})\mathrm{M} \tag{44}$$

$$\forall t=0,\dots,T; a\in\mathbf{A}; \omega\in\mathbf{\Omega}$$

$$-\beta_a^{\omega}\mathrm{M} \le \sum_{k\in\mathbf{K}_a}\delta_k^{\omega}(t) \le \beta_a^{\omega}\mathrm{M}, \forall t=0,\dots,T; a\in\mathbf{A}; \omega\in\mathbf{\Omega} \tag{45}$$

When vehicle ω plans to visit arm a in the following time (i.e., $\beta_a^{\omega}=1$), then Eq. (44) is effective and $\sum_{k\in\mathbf{K}_a}\delta_k^{\omega}(t)=1+\sum_{t^{turn}=0}^{\min(t_0,T^{turn})} ta_a^{\omega}\left(t-t^{turn}\right)$. According to the constrain Eq. (43), the gap between two turning-around maneuvers is larger than T^{turn}, which means $\sum_{t^{turn}=0}^{\min(t_0,T^{turn})} ta_a^{\omega}\left(t-t^{turn}\right)$ is equal to 1 only if the vehicle turns around in the last T^{turn} seconds. Otherwise, Eq. (45) is effective and $\sum_{k\in\mathbf{K}_a}\delta_k^{\omega}(t)=0$.

It is assumed that vehicle ω can only change one lane within one time step. That is, if vehicle ω is in lane k_1 at time step t (i.e., $\delta_{k_1}^{\omega}(t)=1$), then it can only take its current or adjacent lanes at time step $t+1$:

$$\begin{aligned} &\delta_{k_1}^{\omega}(t)-1 \le \delta_{k_2}^{\omega}(t+1) \le 1-\delta_{k_1}^{\omega}(t) \\ &\forall t=0,\dots,T-1; k_1,k_2\in\mathbf{K}_a, \left|k_2-k_1\right|\ge 2; a\in\mathbf{A}_0^{\omega}; \omega\in\mathbf{\Omega} \end{aligned} \tag{46}$$

Eq. (46) sets $\delta_{k_2}^{\omega}(t+1)=0$ when $\delta_{k_1}^{\omega}(t)=0$ and $\left|k_2-k_1\right|\ge 2$. That is, vehicle ω cannot change more than one lanes within one time step.

If vehicle ω is idling during time step $t+1$ (i.e., $x_a^{\omega}(t)=x_a^{\omega}(t+1)$), then it cannot change lanes and should remain in its current lane (i.e., $\delta_k^{\omega}(t)=\delta_k^{\omega}(t+1)$):

$$\begin{aligned} &-\mathrm{M}\left(x_a^{\omega}(t)-x_a^{\omega}(t+1)\right) \le \delta_k^{\omega}(t)-\delta_k^{\omega}(t+1) \le \mathrm{M}\left(x_a^{\omega}(t)-x_a^{\omega}(t+1)\right) \\ &\forall t=0,\dots,T-1; k\in\mathbf{K}_a; a\in\mathbf{A}_0^{\omega}; \omega\in\mathbf{\Omega} \end{aligned} \tag{47}$$

To avoid blocking incoming vehicles, the lane in which vehicle ω leaves the control zone is constrained as:

$$\bar{\mu}_a^{\omega}(t)-1 \le \sum_{k\in\mathbf{K}_{out}^{\omega}}\delta_k^{\omega}(t)-1 \le 1-\bar{\mu}_a^{\omega}(t), \forall t=0,\dots,T; a=a_{out}^{\omega}; \omega\in\mathbf{\Omega} \tag{48}$$

where $\mathbf{K}_{out}^{\omega}$ is the set of lanes vehicle ω can use to leave the control zone in the destination arm a_{out}^{ω}. Eq. (48) guarantees that vehicle ω leaves the control zone in one lane of $\mathbf{K}_{out}^{\omega}$ (i.e., $\sum_{k\in\mathbf{K}_{out}^{\omega}}\delta_k^{\omega}(t)=1$ when $\bar{\mu}_a^{\omega}(t)=1$).

Two lanes are occupied during the whole process of turning around. When vehicle ω turns around from its left side, the currently occupied lane and its left adjacent lane of the driving direction are occupied. They are realized by Eqs. (49) and (50).

$$\begin{aligned} &2-\mathrm{M}\left(3-\delta_{k^{left}}^{\omega}(t-t^{turn})-\delta_k^{\omega}(t-t^{turn})-tal_a^{\omega}(t-t^{turn})+dir_a^{\omega}(t)\right) \le \delta_{k^{left}}^{\omega}(t)+\delta_k^{\omega}(t) \\ &\le 2+\mathrm{M}\left(3-\delta_{k^{left}}^{\omega}(t-t^{turn})-\delta_k^{\omega}(t-t^{turn})-tal_a^{\omega}(t-t^{turn})+dir_a^{\omega}(t)\right) \\ &\forall t=0,\dots,T-1; \omega\in\mathbf{\Omega}; k\in\mathbf{K}_a\backslash\{k_a^{left}\}; t^{turn}=0,\dots,\min(t_0,T^{turn}); a\in\mathbf{A} \end{aligned} \tag{49}$$

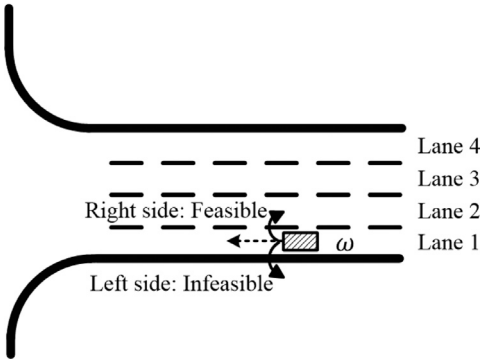

Fig. 5. Illustration of infeasible turning around from the left side.

$$2-\mathrm{M}\left(4-\delta^{\omega}_{k^{right}}(t-t^{turn})-\delta^{\omega}_{k}(t-t^{turn})-tal^{\omega}_{a}(t-t^{turn})-dir^{\omega}_{a}(t)\right)\le\delta^{\omega}_{k^{right}}(t)+\delta^{\omega}_{k}(t)$$
$$\le 2+\mathrm{M}\left(4-\delta^{\omega}_{k^{right}}(t-t^{turn})-\delta^{\omega}_{k}(t-t^{turn})-tal^{\omega}_{a}(t-t^{turn})-dir^{\omega}_{a}(t)\right) \quad (50)$$
$$\forall t=0,\dots,T-1;\omega\in\mathbf{\Omega};k\in\mathbf{K}_a\backslash\{k^{right}_a\};t^{turn}=0,\dots,\min(t_0,T^{turn});a\in\mathbf{A}$$

$$2-\mathrm{M}\left(3-\delta^{\omega}_{k^{right}}(t-t^{turn})-\delta^{\omega}_{k}(t-t^{turn})-tar^{\omega}_{a}(t-t^{turn})+dir^{\omega}_{a}(t)\right)\le\delta^{\omega}_{k^{right}}(t)+\delta^{\omega}_{k}(t)$$
$$\le 2+\mathrm{M}\left(3-\delta^{\omega}_{k^{right}}(t-t^{turn})-\delta^{\omega}_{k}(t-t^{turn})-tar^{\omega}_{a}(t-t^{turn})+dir^{\omega}_{a}(t)\right) \quad (51)$$
$$\forall t=0,\dots,T-1;\omega\in\mathbf{\Omega};k\in\mathbf{K}_a\backslash\{k^{right}_a\};t^{turn}=0,\dots,\min(t_0,T^{turn});a\in\mathbf{A}$$

$$2-\mathrm{M}\left(4-\delta^{\omega}_{k^{left}}(t-t^{turn})-\delta^{\omega}_{k}(t-t^{turn})-tar^{\omega}_{a}(t-t^{turn})-dir^{\omega}_{a}(t)\right)\le\delta^{\omega}_{k^{left}}(t)+\delta^{\omega}_{k}(t)$$
$$\le 2+\mathrm{M}\left(4-\delta^{\omega}_{k^{left}}(t-t^{turn})-\delta^{\omega}_{k}(t-t^{turn})-tar^{\omega}_{a}(t-t^{turn})-dir^{\omega}_{a}(t)\right) \quad (52)$$
$$\forall t=0,\dots,T-1;\omega\in\mathbf{\Omega};k\in\mathbf{K}_a\backslash\{k^{left}_a\};t^{turn}=0,\dots,\min(t_0,T^{turn});a\in\mathbf{A}$$

In Eqs. (49) and (50), $tal^{\omega}_{a}(t)$ is an auxiliary variable. $tal^{\omega}_{a}(t)=1$ if vehicle ω turns around from its left side in arm a at time t; $tal^{\omega}_{a}(t)=0$, otherwise. k^{left} is the left adjacent lane of lane k when facing the stop line as shown in Fig. 4. k^{right} is the right adjacent lane of lane k when facing the stop line. k^{left}_a and k^{right}_a indicates the leftmost lane and the rightmost lanes of the link part of arm a.

Similarly, the currently occupied lane and the right adjacent lane of the driving direction are occupied when a vehicle turns around from its right side. It is constrained by Eqs. (51) and (52), in which $tar^{\omega}_{a}(t)$ is an auxiliary variable. $tar^{\omega}_{a}(t)=1$ if vehicle ω turns around from its right side in arm a at time step t; $tar^{\omega}_{a}(t)=0$, otherwise.

There is no doubt that vehicles have to turn around from either its left side or its right side:

$$tar^{\omega}_{a}(t)+tal^{\omega}_{a}(t)=ta^{\omega}_{a}(t),\forall t=0,\dots,T;\omega\in\mathbf{\Omega};a\in\mathbf{A} \quad (53)$$

where $ta^{\omega}_{a}(t)$ is an auxiliary variable. $ta^{\omega}_{a}(t)=1$ if vehicle ω turns around in arm a at time step t; $ta^{\omega}_{a}(t)=0$, otherwise.

However, vehicles cannot turn around from its left or right side in some cases. For instance, a vehicle cannot turn around from the left side when it drives toward the stop bar in the leftmost lane of the arm, as shown in Fig. 5. This is guaranteed by:

$$-\mathrm{M}\left(1-\delta^{\omega}_{k}(t)+dir^{\omega}_{a}(t)\right)\le tal^{\omega}_{a}(t)\le\mathrm{M}\left(1-\delta^{\omega}_{k}(t)+dir^{\omega}_{a}(t)\right)$$
$$\forall t=0,\dots,T;\omega\in\mathbf{\Omega};k=k^{left}_a;a\in\mathbf{A} \quad (54)$$

$$-\mathrm{M}\left(2-\delta^{\omega}_{k}(t)-dir^{\omega}_{a}(t)\right)\le tal^{\omega}_{a}(t)\le\mathrm{M}\left(2-\delta^{\omega}_{k}(t)-dir^{\omega}_{a}(t)\right)$$
$$\forall t=0,\dots,T;\omega\in\mathbf{\Omega};k=k^{right}_a;a\in\mathbf{A} \quad (55)$$

$$-\mathrm{M}\left(1-\delta^{\omega}_{k}(t)+dir^{\omega}_{a}(t)\right)\le tar^{\omega}_{a}(t)\le\mathrm{M}\left(1-\delta^{\omega}_{k}(t)+dir^{\omega}_{a}(t)\right)$$
$$\forall t=0,\dots,T;\omega\in\mathbf{\Omega};k=k^{right}_a;a\in\mathbf{A} \quad (56)$$

$$-\mathrm{M}\left(2-\delta^{\omega}_{k}(t)-dir^{\omega}_{a}(t)\right)\le tar^{\omega}_{a}(t)\le\mathrm{M}\left(2-\delta^{\omega}_{k}(t)-dir^{\omega}_{a}(t)\right)$$
$$\forall t=0,\dots,T;\omega\in\mathbf{\Omega};k=k^{left}_a;a\in\mathbf{A} \quad (57)$$

Eqs. (54) and (55) indicate the cases in which vehicle ω cannot turn around from the left side. Eqs. (56) and (57) indicate the cases in which vehicle ω cannot turn around from the right side.

Note that we assume two lanes are occupied for a U-turn maneuver for simplification. But it is not difficult to modify the constraints (Eqs. (44), (46), (49)–(52), (54)–(57)) if more occupied lanes (e.g., three lanes) are needed.

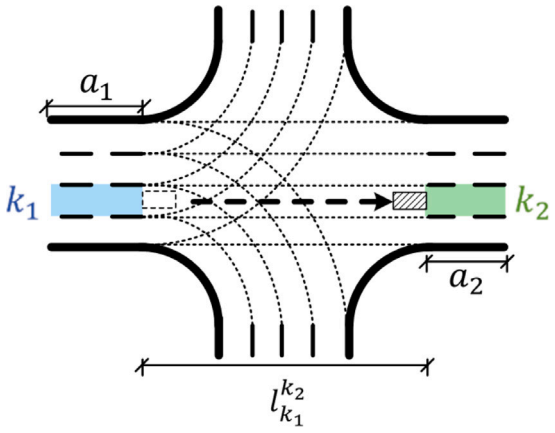

Fig. 6. Illustration of a vehicle entering an arm.

3.1.6. Entering an arm

The constraints of entering an arm deal with the lane choice and the entering time point when a vehicle enters a new arm. If vehicle ω plans to travel from arm a_1 to arm a_2 (i.e., $\gamma_{a_1,a_2}^{\omega}=1$), then the entering time $\underline{t}_{a_2}^{\omega}$ is determined by the leaving time $\bar{t}_{a_1}^{\omega}$ and the travel time in the connectors within the intersection area as shown in Fig. 6:

$$\begin{aligned}&-\mathrm{M}\left(2-\gamma_{a_1,a_2}^{\omega}-\delta_{k_1}^{\omega}(T)\right)\le \underline{t}_{a_2}^{\omega}-\left(\bar{t}_{a_1}^{\omega}+\frac{l_{k_1}^{k_2}}{v_{k_1}^{k_2}}\right)\le \mathrm{M}\left(2-\gamma_{a_1,a_2}^{\omega}-\delta_{k_1}^{\omega}(T)\right)\\&\forall k_2=k_{1+}^{a_2};k_1\in\mathbf{K}_{a_1}^{a_2};a_1,a_2\in\mathbf{A}_0^{\omega};\omega\in\mathbf{\Omega}\end{aligned}\tag{58}$$

The last time step T is used in Eq. (58) to indicate the lane in which vehicle ω leaves, the same as Eq. (11). $l_{k_1}^{k_2}$ and $v_{k_1}^{k_2}$ are the length and travel speed in connector $\langle k_1,k_2\rangle$.

Further, the lane in which vehicle ω enters arm a_2 is determined by the lane in which vehicle ω leaves the link part of arm a_1:

$$\gamma_{a_1,a_2}^{\omega}-1\le\delta_{k_2}^{\omega}(0)-\delta_{k_1}^{\omega}(T)\le 1-\gamma_{a_1,a_2}^{\omega},\forall k_2=k_{1+}^{a_2};k_1\in\mathbf{K}_{a_1}^{a_2};a_1,a_2\in\mathbf{A}_0^{\omega};\omega\in\mathbf{\Omega}\tag{59}$$

Eq. (59) indicates that vehicle ω will enter arm a_2 in lane k_2 if it leaves the link part of arm a_1 in lane k_1 (i.e., $\delta_{k_2}^{\omega}(0)=\delta_{k_1}^{\omega}(T)$ when $\gamma_{a_1,a_2}^{\omega}=1$).

Vehicles are not permitted to change lanes when entering an arm. If vehicle ω enters arm a_2 during time step $t+1$ (i.e., $\underline{\mu}_a^{\omega}(t)=0$ and $\underline{\mu}_a^{\omega}(t+1)=1$), its lane choice should keep the same (i.e., $\delta_k^{\omega}(t)=\delta_k^{\omega}(t+1)$):

$$\begin{aligned}&-\left(1+\underline{\mu}_a^{\omega}(t)-\underline{\mu}_a^{\omega}(t+1)\right)\le\delta_k^{\omega}(t)-\delta_k^{\omega}(t+1)\le 1+\underline{\mu}_a^{\omega}(t)-\underline{\mu}_a^{\omega}(t+1)\\&\forall t=0,\dots,T-1;k\in\mathbf{K}_a;a\in\mathbf{A}^{\omega};\omega\in\mathbf{\Omega}\end{aligned}\tag{60}$$

$\underline{\mu}_a^{\omega}(t)$ is an auxiliary variable for the convenience of modeling. It is related to $\underline{t}_a^{\omega}$ in the following Eq. (61):

$$-\mathrm{M}\left(1-\underline{\mu}_a^{\omega}(t)\right)\le t\cdot\Delta t-\underline{t}_a^{\omega}\le \mathrm{M}\underline{\mu}_a^{\omega}(t),\forall t=0,\dots,T;a\in\mathbf{A};\omega\in\mathbf{\Omega}\tag{61}$$

Eq. (61) indicates that $\underline{\mu}_a^{\omega}(t)=1$ if $t\cdot\Delta t\ge\underline{t}_a^{\omega}$; $\underline{\mu}_a^{\omega}(t)=0$, otherwise.

3.1.7. Leaving the link part of an arm

The constraints of leaving the link part of an arm deal with the selection of lanes available for a vehicle to travel from a preceding arm to a following arm. If vehicle ω leaves the link part of a non-destination arm $a\ne a_{out}^{\omega}$ during time step $t+1$ (i.e., $\bar{\mu}_a^{\omega}(t)=0$ and $\bar{\mu}_a^{\omega}(t+1)=1$) as shown in Fig. 3(c), then $x_a^{\omega}(t)\ge 0$ and $x_a^{\omega}(t+1)<0$. The above Eqs. (8) and (9) guarantee that $x_a^{\omega}(t)\ge 0$ when $\bar{\mu}_a^{\omega}(t)=0$. Eq. (10) guarantees that $x_a^{\omega}(t+1)<0$ when $\bar{\mu}_a^{\omega}(t+1)=1$. If vehicle ω leaves the link part of the destination arm a_{out}^{ω} during time step $t+1$ as shown in Fig. 3(d), then $L_a\ge x_a^{\omega}(t)\ge 0$ and $x_a^{\omega}(t+1)\ge L_a$ are guaranteed by Eqs. (8), (9), and (12).

When vehicle ω leaves the link part of a non-destination arm $a_1\ne a_{out}^{\omega}$, the selected lane is constrained as:

$$\gamma_{a_1,a_2}^{\omega}-1\le\sum_{k\in\mathbf{K}_{a_1}^{a_2}}\delta_k^{\omega}(T)-1\le 1-\gamma_{a_1,a_2}^{\omega},\forall a_1,a_2\in\mathbf{A}_0^{\omega},a_1\ne a_{out}^{\omega};\omega\in\mathbf{\Omega}\tag{62}$$

If vehicle ω plans to travel from arm $a_1\ne a_{out}^{\omega}$ to arm a_2 (i.e., $\gamma_{a_1,a_2}^{\omega}=1$), then one lane in $\mathbf{K}_{a_1}^{a_2}$ is used. On the other hand, $\gamma_{a_1,a_2}^{\omega}=0$ if arm a_1 and arm a_2 are not connected by connectors (i.e., $\mathbf{K}_{a_1}^{a_2}=\emptyset$), which is guaranteed by Eq. (23).

$\bar{\mu}_a^{\omega}(t)$ is an auxiliary binary variable for the convenience of modeling. It is related to $\bar{t}_a^{\omega}$ in the following Eq. (63):

$$-\mathrm{M}\left(1-\bar{\mu}_a^{\omega}(t)\right) \le t\cdot\Delta t-\bar{t}_a^{\omega} \le \mathrm{M}\bar{\mu}_a^{\omega}(t), \forall t=0,\dots,T; a\in\mathbf{A}; \omega\in\mathbf{\Omega} \tag{63}$$

Eq. (63) indicates that $\bar{\mu}_a^{\omega}(t)=1$ if $t\cdot\Delta t\ge\bar{t}_a^{\omega}$; $\bar{\mu}_a^{\omega}(t)=0$, otherwise.

3.1.8. No lane changing zone

According to the assumptions, vehicles cannot change lanes within the intersection area, which are guaranteed by the constraints of no lane changing zones. If vehicle ω travels in the connector part of a non-destination arm within the intersection area or outside the control zone in the destination arm (i.e., $\bar{\mu}_a^{\omega}(t+1)=1$), then vehicle ω is constrained not to change lanes:

$$\delta_k^{\omega}(t+1)-\delta_k^{\omega}(t)\le 1-\bar{\mu}_a^{\omega}(t+1), \forall t=0,\dots,T-1; k\in\mathbf{K}_a; a\in\mathbf{A}_0^{\omega}; \omega\in\mathbf{\Omega} \tag{64}$$

Eq. (64) guarantees that $\delta_k^{\omega}(t+1)=\delta_k^{\omega}(t)$ when $\bar{\mu}_a^{\omega}(t+1)=1$.

3.1.9. Spatial safety gaps

The constraints of spatial safety gaps guarantee the safety between a preceding vehicle and a following vehicle traveling in the same lane in the link part of an arm. When two vehicles travel in the same lane in the same arm, a spatial gap d should be applied for safety concerns:

$$\left|x_a^{\omega_2}(t)-x_a^{\omega_1}(t)\right| \ge d-\mathrm{M}\left(1-\rho_a^{\omega_1,\omega_2}(t)\right), \forall t=0,\dots,T; a\in\mathbf{A}_0^{\omega_1}\cap\mathbf{A}_0^{\omega_2}; \omega_1,\omega_2\in\mathbf{\Omega} \tag{65}$$

where $\rho_a^{\omega_1,\omega_2}(t)$ is an auxiliary binary variable. $\rho_a^{\omega_1,\omega_2}(t)=1$ if vehicle ω_1 and vehicle ω_2 travel in the same lane (i.e., $\sum_{k\in\mathbf{K}_a}\left|\delta_k^{\omega_1}(t)-\delta_k^{\omega_2}(t)\right|=0$) in the link part of arm a at time step t (i.e., $\underline{\mu}_a^{\omega_1}(t)=\underline{\mu}_a^{\omega_2}(t)=1$ and $\bar{\mu}_a^{\omega_1}(t)=\bar{\mu}_a^{\omega_2}(t)=0$). In that case, Eq. (65) is effective. $\rho_a^{\omega_1,\omega_2}(t)$ is constrained by

$$\begin{aligned}&\underline{\mu}_a^{\omega_1}(t)-\bar{\mu}_a^{\omega_1}(t)+\underline{\mu}_a^{\omega_2}(t)-\bar{\mu}_a^{\omega_2}(t)-\sum_{k\in\mathbf{K}_a}\left|\delta_k^{\omega_1}(t)-\delta_k^{\omega_2}(t)\right|-1\le\rho_a^{\omega_1,\omega_2}(t)\\&\forall t=0,\dots,T; a\in\mathbf{A}_0^{\omega_1}\cap\mathbf{A}_0^{\omega_2}; \omega_1,\omega_2\in\mathbf{\Omega}\end{aligned} \tag{66}$$

Eq. (66) guarantees that $\rho_a^{\omega_1,\omega_2}(t)=1$ when $\underline{\mu}_a^{\omega_1}(t)=\underline{\mu}_a^{\omega_2}(t)=1$, $\bar{\mu}_a^{\omega_1}(t)=\bar{\mu}_a^{\omega_2}(t)=0$, and $\sum_{k\in\mathbf{K}_a}\left|\delta_k^{\omega_1}(t)-\delta_k^{\omega_2}(t)\right|=0$. Note that $\rho_a^{\omega_1,\omega_2}(t)$ is unconstrained (i.e., $\rho_a^{\omega_1,\omega_2}(t)$ is not necessarily zero) if vehicle ω_1 and vehicle ω_2 travel in different lanes, which can still disable constraint (65).

3.1.10. Temporal safety gaps

The constraints of temporal safety gaps guarantee the safety between a preceding vehicle and a following vehicle diverging at the stop line. When two vehicles consecutively pass the stop line location in the same lane in arm $a\ne a_{out}^{\omega}$, a temporal gap τ is applied between their passing times for safety concerns:

$$\begin{aligned}&\left|\bar{t}_a^{\omega_1}-\bar{t}_a^{\omega_2}\right|\ge\tau-\mathrm{M}\left(2-\beta_a^{\omega_1}-\beta_a^{\omega_2}+\sum_{k\in\mathbf{K}_a}\left|\delta_k^{\omega_1}(T)-\delta_k^{\omega_2}(T)\right|\right)\\&\forall a\in\mathbf{A}_0^{\omega_1}\cap\mathbf{A}_0^{\omega_2}, a\ne a_{out}^{\omega}; \omega_1,\omega_2\in\mathbf{\Omega}\end{aligned} \tag{67}$$

Eq. (67) is set to avoid diverging conflicts as shown in Fig. 7. Eq. (67) is effective if vehicle ω_1 and vehicle ω_2 both plan to visit arm a (i.e., $\beta_a^{\omega_1}=\beta_a^{\omega_2}=1$) and leave the link part in the same lane (i.e., $\sum_{k\in\mathbf{K}_a}\left|\delta_k^{\omega_1}(T)-\delta_k^{\omega_2}(T)\right|=0$).

3.1.11. Collision avoidance within intersection areas

The constraints of collision avoidance within intersection areas guarantee the safety between conflicting vehicles within the intersection area.

Suppose vehicle ω_1 plans to travel from lane k_1 in arm a_1 to lane k_2 in arm a_2 via connector $\langle k_1,k_2\rangle$ (i.e., $\gamma_{a_1,a_2}^{\omega_1}=\delta_{k_1}^{\omega_1}(T)=1$) and vehicle ω_2 plans to travel from lane k_3 in arm a_3 to lane k_4 in arm a_4 via connector $\langle k_3,k_4\rangle$ (i.e., $\gamma_{a_3,a_4}^{\omega_2}=\delta_{k_3}^{\omega_2}(T)=1$) as shown in Fig. 8. There is a conflict point between connector $\langle k_1,k_2\rangle$ and connector $\langle k_3,k_4\rangle$. For safety concerns, a temporal gap τ is applied between their passing times at the conflict point.

$$\begin{aligned}&\left|\left(\bar{t}_{a_1}^{\omega_1}+\frac{l_{k_1,k_2}^{p}}{v_{k_1}^{k_2}}\right)-\left(\bar{t}_{a_3}^{\omega_2}+\frac{l_{k_3,k_4}^{p}}{v_{k_3}^{k_4}}\right)\right|\ge\tau-\mathrm{M}\left(4-\gamma_{a_1,a_2}^{\omega_1}-\delta_{k_1}^{\omega_1}(T)-\gamma_{a_3,a_4}^{\omega_2}-\delta_{k_3}^{\omega_2}(T)\right)\\&\forall p\in\mathbf{P}_{k_1,k_2}^{k_3,k_4}; k_3\in\mathbf{K}_{a_3}^{a_4}, k_4=k_{3+}^{a_4}; k_1\in\mathbf{K}_{a_1}^{a_2}, k_2=k_{1+}^{a_2};\\&a_1,a_2\in\mathbf{A}_0^{\omega_1}, a_3,a_4\in\mathbf{A}_0^{\omega_2}, a_4\ne a_1, a_3\ne a_2; \omega_1,\omega_2\in\mathbf{\Omega}\end{aligned} \tag{68}$$

In Eq. (68), $\mathbf{P}_{k_1,k_2}^{k_3,k_4}$ is the set of conflict points between connector $\langle k_1,k_2\rangle$ and connector $\langle k_3,k_4\rangle$, which may have more than one points for a general case; l_{k_1,k_2}^{p} is the distance between the start of connector $\langle k_1,k_2\rangle$ and conflict point p.

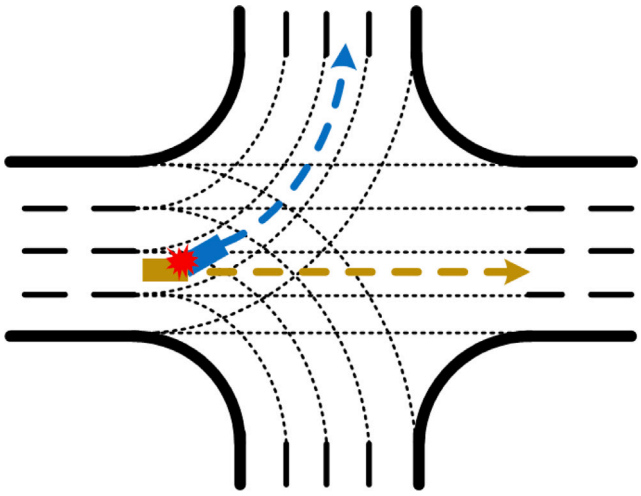

Fig. 7. Illustration of diverging conflicts.

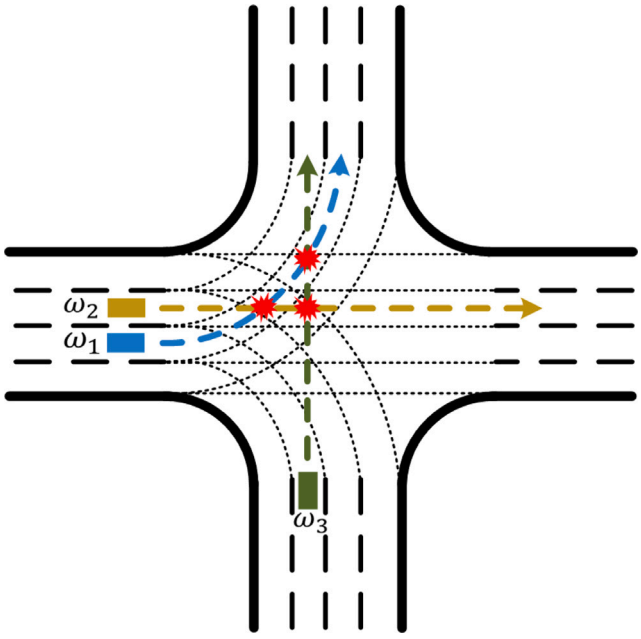

Fig. 8. Conflicts within the intersection area.

Besides Eq. (68), another case needs special attention. Suppose vehicle ω_1 plans to travel from lane k_1 in arm a_1 to lane k_2 in arm a_2 via connector $\langle k_1, k_2 \rangle$ and vehicle ω_2 plans to travel from lane k_2 in arm a_2 to lane k_1 in arm a_1 via connector $\langle k_2, k_1 \rangle$. In that case, there are countless conflict points in $\mathbf{P}_{k_1,k_2}^{k_3,k_4}$, which cannot be covered by constraints (68) as shown in Fig. 9. The following Eqs. (69) and (70) are applied instead:

$$\begin{aligned} &\bar{t}_{a_1}^{\omega_1} - \underline{t}_{a_1}^{\omega_2} \geq \tau - \mathrm{M}\left(4 - \gamma_{a_1,a_2}^{\omega_1} - \delta_{k_1}^{\omega_1}(T) - \gamma_{a_2,a_1}^{\omega_2} - \delta_{k_2}^{\omega_2}(T) + \pi_{k_1,k_2}^{\omega_1,\omega_2}\right) \\ &\forall k_1 \in \mathbf{K}_{a_1}^{a_2}, k_2 = k_{1+}^{a_2}; a_1, a_2 \in \mathbf{A}_0^{\omega_1} \cap \mathbf{A}_0^{\omega_2}; \omega_1, \omega_2 \in \boldsymbol{\Omega} \end{aligned} \tag{69}$$

$$\begin{aligned} &\bar{t}_{a_2}^{\omega_2} - \underline{t}_{a_2}^{\omega_1} \geq \tau - \mathrm{M}\left(5 - \gamma_{a_1,a_2}^{\omega_1} - \delta_{k_1}^{\omega_1}(T) - \gamma_{a_2,a_1}^{\omega_2} - \delta_{k_2}^{\omega_2}(T) - \pi_{k_1,k_2}^{\omega_1,\omega_2}\right) \\ &\forall k_1 \in \mathbf{K}_{a_1}^{a_2}, k_2 = k_{1+}^{a_2}; a_1, a_2 \in \mathbf{A}_0^{\omega_1} \cap \mathbf{A}_0^{\omega_2}; \omega_1, \omega_2 \in \boldsymbol{\Omega} \end{aligned} \tag{70}$$

where $\pi_{k_1,k_2}^{\omega_1,\omega_2}$ is an auxiliary binary variable. $\pi_{k_1,k_2}^{\omega_1,\omega_2} = 0$ if vehicle ω_1 enters connector $\langle k_1, k_2 \rangle$ after vehicle ω_2 leaves connector $\langle k_2, k_1 \rangle$ (i.e., $\bar{t}_{a_1}^{\omega_1} > \underline{t}_{a_1}^{\omega_2}$); $\pi_{k_1,k_2}^{\omega_1,\omega_2} = 1$, otherwise. Eq. (69) is effective when $\pi_{k_1,k_2}^{\omega_1,\omega_2} = 0$ and Eq. (70) is effective when $\pi_{k_1,k_2}^{\omega_1,\omega_2} = 1$.

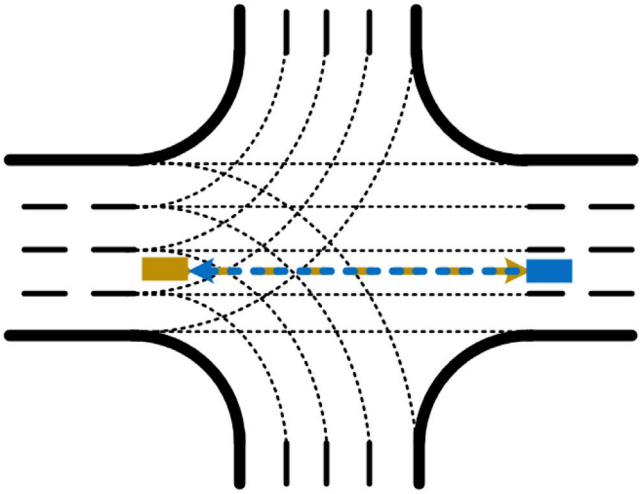

Fig. 9. Illustration of collision in the same connector.

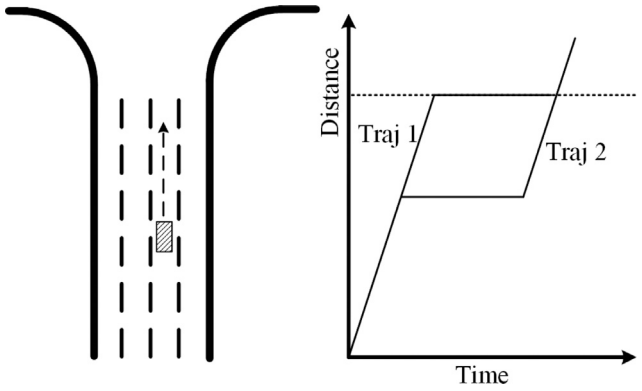

Fig. 10. Illustration of multiple trajectory solutions.

3.2. Objective function

The objective of the optimization model is to minimize total vehicle delay. Vehicle delay is defined as the difference between the actual travel time and the free-flow travel time. The actual travel time is calculated as the difference between the time points when a vehicle is generated and leaves the control zone. Both the delays outside and inside the control zone are included. The free-flow travel time is determined by the movement of each vehicle. Therefore, minimizing vehicle delay is equivalent to minimizing the vehicle's leaving time as the generation time is a constant. The objective function is formulated as

$$\min \sum_{\omega \in \Omega} \bar{t}^{\omega}_{a^{\omega}_{out}} \tag{71}$$

where $\bar{t}^{\omega}_{a^{\omega}_{out}}$ is the time when vehicle ω leaves the link part of the destination arm a^{ω}_{out}, which means leaving the control zone. However, multiple optimal trajectory solutions may exist in terms of total vehicle delay. And the vehicle trajectories of certain solutions are unfavorable. For example, the two trajectories in Fig. 10 have the same delay. But the second trajectory blocks traffic in the middle of the arm and the first trajectory is preferred. To this end, a secondary objective is added:

$$\min \sum_{\omega \in \Omega} \sum_{\substack{a \in \mathbf{A}^{\omega}_{0} \\ a \neq a^{\omega}_{out}}} \sum_{t=0}^{T} x^{\omega}_{a}(t) \tag{72}$$

Objective function (72) encourages vehicles to avoid blocking incoming vehicles in the middle of arms.

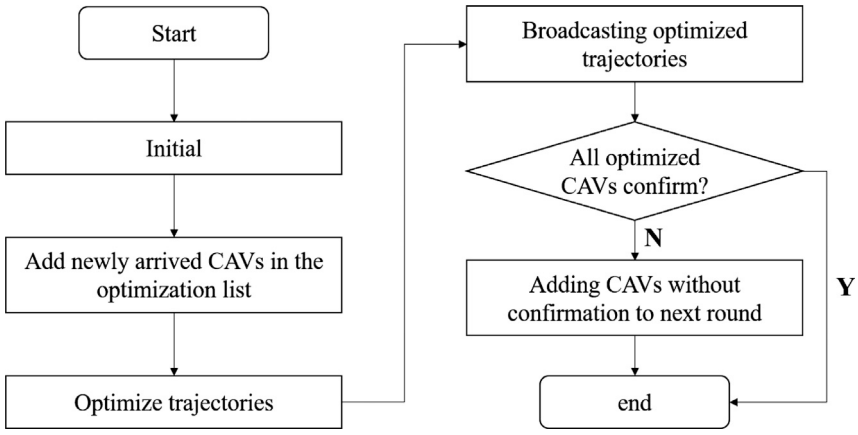

Fig. 11. Working flow of the LAF control.

To combine Eqs. (71) and (72), similar to Yu et al. (2019a), the final objective function is shown as

$$\min w_1 \sum_{\omega \in \mathbf{\Omega}} \tilde{t}^{\omega}_{a^{\omega}_{out}} + w_2 \sum_{\omega \in \mathbf{\Omega}} \sum_{\substack{a \in \mathbf{A}^{\omega}_0 \\ a \neq a^{\omega}_{out}}} \sum_{t=0}^{T} x^{\omega}_a(t) \tag{73}$$

where w_1 and w_2 are weighting parameters and $w_1 \gg w_2$ to guarantee the solution quality. Constraints include Eqs. (1)–(70). It is noted that all constraints are linear except Eqs. (35), (65), (66), (67), and (68) due to the absolute value function. But they can be easily linearized (Yu et al., 2019a). As a result, the proposed model is an MILP model, which can be solved by many commercial solvers.

4. Implementation procedure

There are two main kinds of parameters in the proposed model, namely, geometric parameters of the intersection layout (e.g., lane numbers and link lengths) and traffic parameters (e.g., vehicle states including longitudinal and latitudinal locations). When the proposed model is applied to a specific intersection, the geometric parameters are then determined. But these geometric parameters can differ when the proposed model is applied to another intersection different from the exemplary one in Fig. 1. In each optimization, traffic parameters are fixed. To cater to time-varying traffic conditions, the rolling horizon scheme is used for the dynamic implementation of the proposed model to update traffic parameters, which is a common practice (Yao et al., 2020).

The working flow of the LAF control is shown in Fig. 11. To handle the problem of possible packet loss, a confirmation mechanism is introduced. Newly arrived vehicles are added to the optimization list at each time step. After optimizing the trajectories of all CAVs in the optimization list, the controller broadcasts the planned trajectories. Each CAV in the optimization list needs to send a confirmation message. If the controller does not receive the confirmation message from a CAV in the optimization list, this CAV will be added to the optimization list at the next step with high priority. Further, a buffer zone is set outside the control zone, which is also covered by the communication range, as shown in Fig. 12. When an arrived vehicle enters the buffer zone, the confirmation mechanism is triggered. In this way, each arrived vehicle is guaranteed to have a planned trajectory before entering the control zone and thus the safety is guaranteed. The minimum length of the buffer zone can be determined by the packet loss rate. For example, if the packet loss rate is 0.1% at each time step and the length of the buffer zone is $2V_a\Delta t$, then we have the confidence of $1-(0.1\%)^2 = 99.9999\%$ that the safety can be guaranteed.

As for the "optimize trajectory" part, the optimization flow is designed in detail. The challenge of solving the proposed MILP model lies in the large dimensions as well as the inclusion of both continuous and binary variables. Approximately, the number of the variables increases quadratically with the planning horizon T. The planning horizon T becomes a critical parameter in solving the proposed model. The model will be infeasible if T is too small due to constraint Eq. (17). However, a large T brings an intensive computational burden. An algorithm is designed to adjust T adaptively and embedded in the rolling horizon scheme:

Step 0: Initialize the planning horizon $T = T_0$.
Step 1: Initialize $\mathbf{A}^{\omega} = \mathbf{A}$ for the vehicles in the optimization list.
Step 2: Update $\mathbf{A}^{\omega}$ for all vehicles in the control zone as $\mathbf{A}^{\omega} = \mathbf{A}^{\omega} \setminus \{a^{\omega}_0\}$ if $a^{\omega}_0 \in \mathbf{A}^{\omega}$.
Step 3: Get $\mathbf{A}^{\omega}_0$ for all vehicles in the control zone as $\mathbf{A}^{\omega}_0 = \mathbf{A}^{\omega} \cup \{a^{\omega}_0\}$.
Step 4: Solve the MILP model.
Step 5: If there are no feasible solutions, then update $T = T + 2\Delta T$, where ΔT is the step length for adjusting T. Go to **Step 4**. Otherwise, get the solutions $\tilde{t}^{\omega}_{a^{\omega}_{out}}$ of each vehicle and go to the next step.

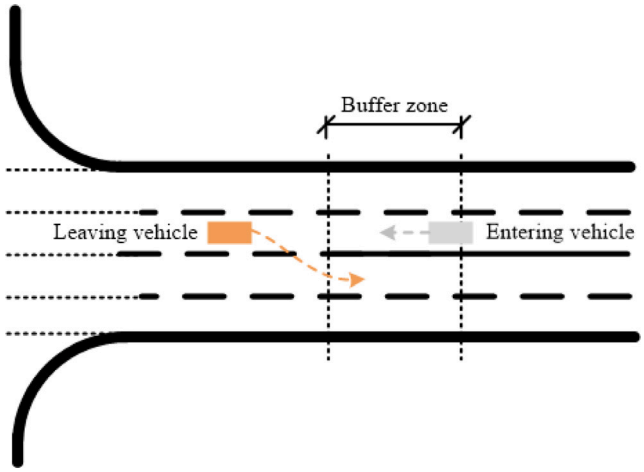

Fig. 12. Setting of a buffer zone to handle packet loss.

Table 2
Basic traffic demand.

Traffic demand (veh/h)	To arm			
From arm	1	2	3	4
1	–	90	150	30
2	30	–	40	50
3	150	30	–	90
4	40	50	20	–

Table 3
Main parameters.

Parameter	Value	Parameter	Value	Parameter	Value
Δt	0.5 s	T_0	30	ΔT	2
L_a	50 m	V_a	10 m/s	τ	1.5 s
d	5 m	w_1	300	w_2	1

Step 6: Update $T = \max\left(\left\lceil \frac{\max_{\omega\in\Omega} \bar{t}^{\omega}_{a^{\omega}_{out}}}{\Delta T} \right\rceil, T - \Delta T\right)$, where $\lceil\cdot\rceil$ is the ceiling function that maps a real number to the least integer greater than or equal to the number.

5. Numerical studies

5.1. Experiment design

To explore the benefits of the proposed LAF control, this study employs the isolated intersection without lane allocation in Fig. 1. The length of the control zone is set as 150 m, which is within the communication range (Chen et al., 2017). Each lane can be used as both approaching and exit lanes for left-turn, through and right-turn vehicles. Vehicles can take flexible routes by way of multiple arms to pass through the intersection. The basic demand of each movement is shown in Table 2, which is scaled proportionally by a demand factor α as the input demand. The critical intersection volume-to-capacity (v/c) ratio (Transportation Research Board (TRB), 2010) of the basic demand is 0.25, which is calculated as the sum of the critical v/c ratio of each phase with maximum phase green times. Left-turn, through and right-turn vehicles are taken into consideration. Low, medium, and high demand levels are tested with $\alpha = 1$, 2, and 4, respectively, which means the v/c ratios of the low, medium and high demand levels are 0.25, 0.5, and 1, respectively. The geometric parameters $l^{k_2}_{k_1}$ and $l^{p}_{k_1,k_2}$ can be easily determined based on the intersection layout. The design speed $v^{k_2}_{k_1}$ in a connector is 8 m/s for left-turn vehicles, 10 m/s for through vehicles, and 6 m/s for right-turn vehicles. Other main parameters are summarized in Table 3.

Two existing solutions, vehicle-actuated control and the ALAF control in the previous study (Yu et al., 2019a), are applied as the benchmarks. In the vehicle-actuated control, the lane allocation in Fig. 13 and three signal phases are used. Phase 1 includes the left-turn vehicles in arm 1 and arm 3. Phase 2 includes the through and the right-turn vehicles in arm 1 and arm 3. Phase 3 includes the left-turn, through, and right-turn vehicles in arm 2 and arm 4. The green extension is 3 s. The all-red clearance time is 3 s. The minimum green time of each phase is 6 s. The maximum green times are 15 s, 30 s, and 20 s for phase 1, phase 2, and

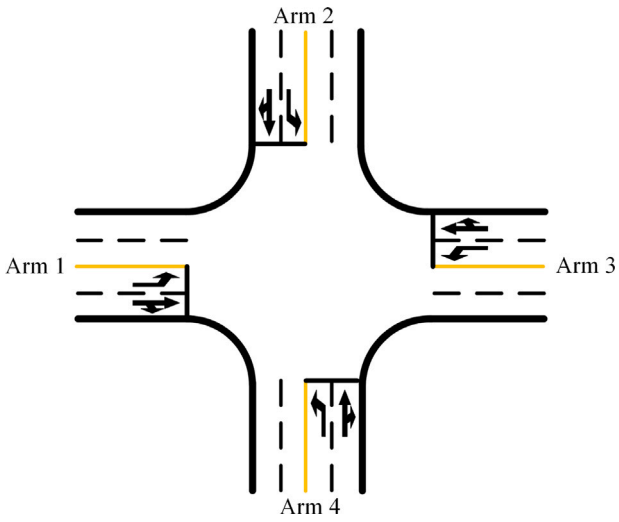

Fig. 13. Lane allocation in vehicle-actuated control.

Table 4
Average vehicle delay (s).

Average vehicle delay	Demand scenarios		
(Standard deviation)	Low ($\alpha = 1$)	Medium ($\alpha = 2$)	High ($\alpha = 4$)
Vehicle-actuated Control	14.50 (3.49)	23.13 (1.95)	34.66 (9.86)
ALAF Control	0.71 (0.09)	0.83 (0.08)	0.91 (0.15)
LAF Control	0.09 (0.07)	0.15 (0.06)	0.28 (0.06)

phase 3, respectively. In the ALAF control, two lanes in each arm are used for approaching lanes and the remaining two are used for exit lanes. That is, the approaching lane allocation in Fig. 13 is removed. The other parameters remain the same as the proposed LAF control for a fair comparison.

The control algorithms are written in C#. The proposed LAF control model is solved using Gurobi 8.1.0 (Gurobi Optimization, Inc., 2019). The model is resolved to plan or update the trajectories of CAVs when newly arrived vehicles enter the control zone. The simulation is conducted in SUMO (Simulation of Urban Mobility) (Krajzewicz et al., 2012) on a server with an Intel 2.4 GHz 12-core CPU with 128 GB memory. Only the trajectories of newly arrived vehicles are optimized for computational efficiency at the cost of system optimality. The trajectories of the vehicles in the control zone that have been optimized in the previous optimization processes are considered in the constraints to avoid collisions. Each optimization is finished within five minutes. Note that computational technologies such as parallel computing and fog computing can be used to greatly improve the computational efficiency. Further, quantum computers may serve as a powerful tool when the fully CAV environment is realized. For example, according to the report in Science (Zhong et al., 2020), the newly developed quantum computer can be 10^{14} faster than using the state-of-the-art supercomputers. The default lane-changing and car-following models in SUMO are used in the vehicle-actuated control. The acceleration/deceleration rates are set as infinity in SUMO so that vehicles can change speeds and lanes instantaneously in the benchmark cases for a fair comparison. Five random seeds are used in the simulation for each demand scenario considering stochastic vehicle arrivals. Each simulation run is 1200 s with a warm-up period of 20 s. (SimulationVideo)

5.2. Results and analysis

To compare the performance of the vehicle-actuated control, the ALAF control, and the proposed LAF control, average vehicle delay and throughput are recorded as the performance measures. The delay of a vehicle is calculated as the difference between the actual travel time and the free-flow travel time of its movement. The actual travel time is calculated as the difference between the time points when a vehicle is generated and leaves the control zone. Both the delays outside and inside the control zone are included. Only the delays of the vehicles that have left the control zone are counted. The simulation results are shown in Tables 4 and 5.

Table 4 shows that the delays increase with the demand when the vehicle-actuated control, the ALAF control, and the LAF control are applied. The average vehicle delay in the vehicle-actuated control rises more noticeably than those in the ALAF control and the LAF control when the demand increases from the low level to the high level. The increased average vehicle delay in the vehicle-actuated control reaches 20.16 s while the values are only 0.20 s and 0.19 s in the ALAF control and the LAF control, respectively. Further, the ALAF control and the LAF control significantly outperform the vehicle-actuated control in terms of average vehicle

Table 5
Vehicle throughput (veh/h).

Throughput	Demand scenarios		
(Standard deviation)	Low ($\alpha = 1$)	Medium ($\alpha = 2$)	High ($\alpha = 4$)
Vehicle-actuated Control	771 (24)	1524 (67)	2638 (110)
ALAF Control	772 (27)	1543 (28)	3069 (36)
LAF Control	778 (18)	1563 (31)	3096 (42)

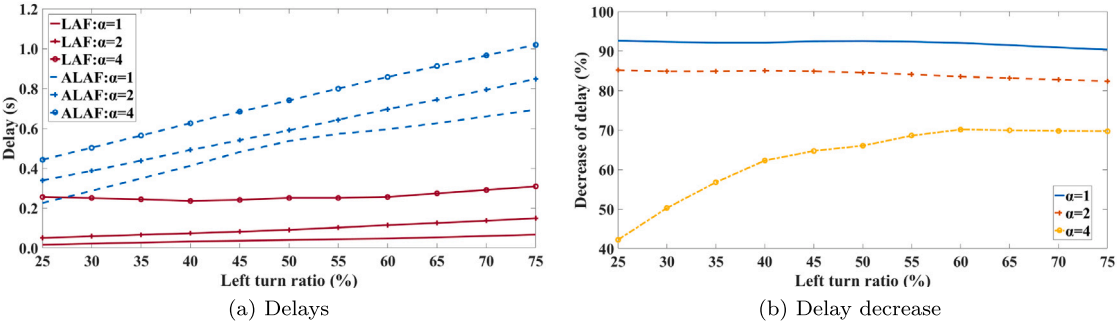

(a) Delays (b) Delay decrease

Fig. 14. Delay results with left-turn ratios.

delays at all demand levels. Compared with the vehicle-actuated control, both the ALAF control and the LAF control reduce average vehicle delays by more than 90%, which validates the benefits of the CAV-based intersection control without lane allocation. It is also observed that the average vehicle delay in the proposed LAF control is less than one third of the one in the ALAF control at each demand level. That is, the proposed LAF control remarkably outperforms the ALAF control in terms of average vehicle delays.

Table 5 shows the vehicle throughput in the vehicle-actuated control, the ALAF control, and the LAF control. At the low and medium demand levels, the throughput of the three control methods differs insignificantly. That means the demands are below the intersection capacity. However, the ALAF control and the LAF control have much higher throughput by ~17% at the high demand level. Because the demand exceeds the intersection capacity in the vehicle-actuated control but is well accommodated in the ALAF control and the LAF control due to the significantly improved capacity. Note that the throughput differs insignificantly in the ALAF control and the LAF control. Higher demand is tested in the following section for further analysis.

5.3. Sensitivity analysis

5.3.1. Demand structures

The delays in the LAF control and the ALAF control with different demand structures (i.e., left-turn ratios) are investigated. The results are shown in Fig. 14(a). The delay in the ALAF control increases noticeably with the growth of traffic demand and the left-turn ratio. In contrast, the delay in the LAF control is not sensitive to the left-turn ratio. Because left-turn vehicles in the LAF control have a shorter shortest path and fewer conflict points on the path as shown as vehicle ω_1 in Fig. 1. In other words, left-turn vehicles are equivalent to right-turn vehicles under the LAF control. The delay decrease in the LAF control compared with the ALAF control is shown in Fig. 14(b). For all tested left-turn ratios, delays can be reduced by at least 40%. It is further observed that the benefits of the LAF control are more significant at the low and the medium demand levels (i.e., $\alpha = 1$ and $\alpha = 2$). Delay is reduced by more than 90% and 80% with all tested left-turn ratios when $\alpha = 1$ and $\alpha = 2$, respectively. And the delay decrease is relatively insensitive to the left-turn ratio. In contrast, the benefits increase noticeably with the increasing left-turn ratio at the high demand level (i.e., $\alpha = 4$). The delay decrease rises from 42% to 67% when the left-turn ratio varies from 25% to 75%.

The throughput in the LAF control and the ALAF control with different demand structures is shown in Fig. 15(a). Different from the delay results, the throughput in the LAF control and the ALAF control differs insignificantly. As discussed in the above section, the input demand is lower than the intersection capacity. As a result, the throughput is expected to equal the input demand and is insensitive to the left-turn ratio. The throughput improvement in the LAF control compared with the ALAF control is depicted in Fig. 15(b). The improvement is less than 4% for all test scenarios. The improvement is very limited especially under low traffic demand. As for the influence of the left-turn ratio, the improvement is lower than in other situations when the left-turn ratio is close to 50%. It is caused by the interference between straight vehicles and left-turn vehicles.

To further explore the performance of the proposed LAF control, higher demand levels ($\alpha = 5, 6, 7, 8$) are tested. The results are shown in Fig. 16. Since the delay in the vehicle-actuated control is significantly larger than the one in the LAF/ALAF control, only the delays in the LAF control and the ALAF control are shown for better illustration. The LAF control outperforms the ALAF control remarkably in terms of vehicle delay at all demand levels. Further, intersection capacity can be observed from Fig. 16 when the throughput lines become flat. For example, the capacity is reached in the vehicle-actuated control when the demand factor α is 4. In contrast, the capacity is still not reached in the LAF control and the ALAF control when α is 8. However, it is observed that the

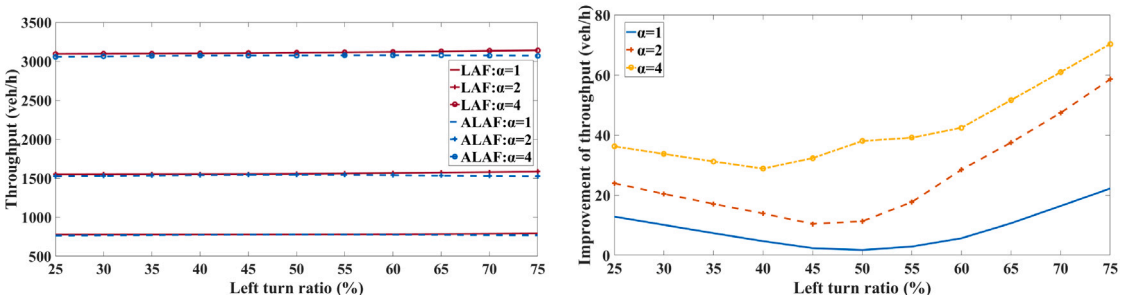

(a) Throughput (b) Throughput improvement

Fig. 15. Throughput results with left-turn ratios.

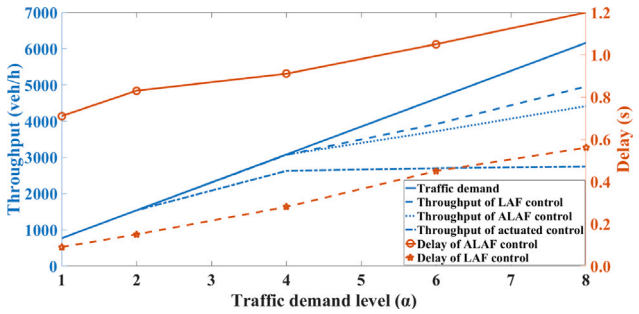

Fig. 16. Comparison between LAF and ALAF control.

throughput line of the ALAF control deviates more from the demand line than the LAF control. That is, the capacity will be reached in the LAF control later than the ALAF control if the demand increases further. Therefore, the LAF control outperforms the ALAF control in terms of both vehicle delay and throughput.

The advantages of the proposed LAF control over the ALAF control mainly come from two factors: (1) The relaxed constraints of defining approaching and exit lanes. Each lane can be used as both an approaching lane and an exit lane as long as safety is guaranteed. As a result, the spatial resources at the intersection can be utilized in a more effective way. (2) Flexible routing. Vehicles can take a detour by way of multiple arms to pass through the intersection if less delay can be achieved. In this way, the solution space of the vehicle trajectory planning is enlarged and potential better solutions are expected.

5.3.2. Temporal safety gaps

The signal-free management method is used in the LAF control and the ALAF control. It means the temporal safety gap is a critical parameter. Because the temporal safety gap can influence control efficiency and safety significantly. Smaller temporal safety gaps may lead to lower delay, but may result in safety problems. The influence of temporal safety gaps on the performance of the LAF control and the ALAF control is investigated. In Bian et al. (2019), 0.5 s is set as the smallest safety gap for constant time headway policy for car-following behaviors under the fully CAV environment. In Li et al. (2010), the time headway is found to be distributed centered on 2.5 s for regular vehicles. In this study, the temporal safety gaps are explored from 0.5 s to 2.5 s per 0.5 s. The results are shown in Fig. 17. The delays under both control methods rise with increasing temporal safety gaps. The LAF control has a much smaller delay than the ALAF control with any temporal safety gap. Besides, the delay line of the LAF control has a smaller slope than the ALAF control when the temporal safety gap is less than 2 s. In other words, the LAF control is more robust to temporal safety gaps when the temporal safety gap is less than 2 s. After the temporal safety gap of 2 s, the delays in both control methods start to increase faster.

6. Conclusion

This paper proposes an MILP model to optimize vehicle trajectories at a “signal-free” intersection without lane allocation under the fully CAV environment. Each lane can be used as both an approaching lane and an exit lane for all vehicle movements including left-turn, through, and right-turn. Vehicles can take flexible routes by way of multiple arms to pass through the intersection. The interactions between vehicle trajectories are modeled explicitly at the microscopic level. Car-following and lane-changing behaviors of the vehicles within the control zone can be optimized in a unified framework in terms of total vehicle delay. In the implementation procedure, the planning horizon is adaptively adjusted to make a balance between the feasibility of the MILP model and computational efficiency. In the numerical studies, only the trajectories of newly arrived vehicles are optimized for

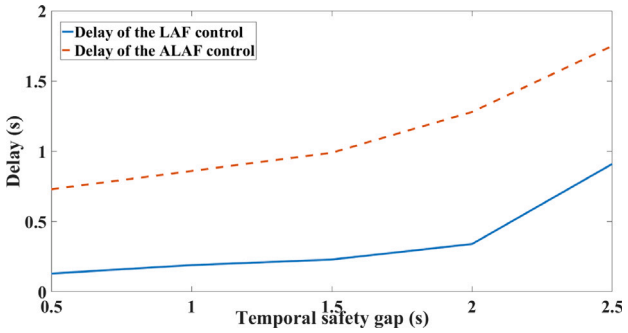

Fig. 17. Sensitivity analysis of temporal safety gaps.

computational efficiency at the cost of system optimality. The simulation results show that the proposed LAF control outperforms the vehicle-actuated control and the ALAF control in the previous study (Yu et al., 2019a) in terms of both vehicle delay and throughput. The sensitivity analysis further validates the advantages of the LAF control over the ALAF control with different demand structures and temporal safety gaps.

This study assumes a fully CAV environment. However, regular vehicles, CVs, and CAVs will coexist in the near future. It is worthwhile to investigate the mixed traffic control at intersections. This study focuses on isolated intersections. It is planned to extend the proposed model to a corridor and a network. For simplification, vehicles are not allowed to change lanes within the intersection area. Flexible trajectories within the intersection area may further enhance the intersection capacity, which will be considered in future research. For simplicity, the first-order vehicle kinematics models are used in this paper. It is not difficult to apply higher-order vehicle kinematics models but the model will be no longer linear. The solving algorithms could be a great challenge. Considering the robustness under stochastic traffic flow is another promising research direction. The computational burden is heavy due to the large dimensions of the model, especially, when the trajectories of all vehicles are optimized at the same time. Efficient algorithms are expected to balance the solution quality and the computational time. Issues such as detection issues may be inevitable even when the fully CAV environment is realized. Data processing methods such as Kalman Filter (Randriamasy et al., 2019) and robust trajectory planning (Sun et al., 2020) can be explored, which is another research direction.

CRediT authorship contribution statement

Ruochen Hao: Methodology, Software, Investigation, Writing – original draft, Writing – review & editing. **Yuxiao Zhang:** Conceptualization, Software, Writing – review & editing. **Wanjing Ma:** Conceptualization, Methodology, Validation, Supervision. **Chunhui Yu:** Supervision, Writing – review & editing, Methodology. **Tuo Sun:** Conceptualization, Supervision. **Bart van Arem:** Supervision, Review.

Data availability

Data will be made available on request

Acknowledgments

This research was funded by National Natural Science Foundation of China (52131204 and 52272336) and Fundamental Research Funds for the Central Universities, China (22120220580 and 1600141335/002). The views presented in this paper are those of the authors alone.

References

Allsop, R.E., 1976. SIGCAP: A computer program for assessing the traffic capacity of signal-controlled road junctions. Traffic Eng. Control 17 (8–9), 338–341, URL https://www.scopus.com/inward/record.uri?eid=2-s2.0-0016986186&partnerID=40&md5=e49ea20eeb87a2204774011ead5ffc86.

Alonso, J., Milanés, V., Pérez, J., Onieva, E., González, C., de Pedro, T., 2011. Autonomous vehicle control systems for safe crossroads. Transp. Res. C 19 (6), 1095–1110. http://dx.doi.org/10.1016/j.trc.2011.06.002, URL http://www.sciencedirect.com/science/article/pii/S0968090X11000921.

Aoki, S., Rajkumar, R., 2022. Cyber traffic light: safe cooperation for autonomous vehicles at dynamic intersections. IEEE Trans. Intell. Transp. Syst. 23 (11), 22519–22534.

Au, T., Stone, P., 2010. Motion planning algorithms for autonomous intersection management. In: Bridging the Gap Between Task and Motion Planning, Papers from the 2010 AAAI Workshop, Atlanta, Georgia, USA, July 11, 2010. In: AAAI Workshops, vol. WS-10-01, AAAI, URL http://aaai.org/ocs/index.php/WS/AAAIW10/paper/view/2053.

Bian, Y., Zheng, Y., Ren, W., Li, S.E., Wang, J., Li, K., 2019. Reducing time headway for platooning of connected vehicles via V2V communication. Transp. Res. C 102, 87–105. http://dx.doi.org/10.1016/j.trc.2019.03.002, URL http://www.sciencedirect.com/science/article/pii/S0968090X18311197.

Campos, G.R., Falcone, P., Wymeersch, H., Hult, R., Sjöberg, J., 2014. Cooperative receding horizon conflict resolution at traffic intersections. In: 53rd IEEE Conference on Decision and Control. IEEE, pp. 2932–2937.

Carlino, D., Boyles, S.D., Stone, P., 2013. Auction-based autonomous intersection management. In: Proc. 16th Int. IEEE Conf. Intelligent Transportation Systems. ITSC 2013, pp. 529–534. http://dx.doi.org/10.1109/ITSC.2013.6728285.

Chen, S., Hu, J., Shi, Y., Peng, Y., Fang, J., Zhao, R., Zhao, L., 2017. Vehicle-to-everything (v2x) services supported by LTE-based systems and 5G. IEEE Commun. Stand. Mag. 1 (2), 70–76. http://dx.doi.org/10.1109/MCOMSTD.2017.1700015.

Dikaiakos, M.D., Florides, A., Nadeem, T., Iftode, L., 2007. Location-aware services over vehicular ad-hoc networks using car-to-car communication. IEEE J. Sel. Areas Commun. 25 (8), 1590–1602.

Dresner, K., Stone, P., 2004. Multiagent traffic management: a reservation-based intersection control mechanism. In: Proc. Third Int. Joint Conf. Autonomous Agents and Multiagent Systems. AAMAS 2004, pp. 530–537.

Dresner, K., Stone, P., 2008. A multiagent approach to autonomous intersection management. J. Artificial Intelligence Res. 31, 591–656.

Feng, Y., Head, K.L., Khoshmagham, S., Zamanipour, M., 2015. A real-time adaptive signal control in a connected vehicle environment. Transp. Res. C 55, 460–473. http://dx.doi.org/10.1016/j.trc.2015.01.007.

Feng, S., Wang, X., Sun, H., Zhang, Y., Li, L., 2018a. A better understanding of long-range temporal dependence of traffic flow time series. Physica A 492, 639–650.

Feng, Y., Yu, C., Liu, H.X., 2018b. Spatiotemporal intersection control in a connected and automated vehicle environment. Transp. Res. C 89, 364–383. http://dx.doi.org/10.1016/j.trc.2018.02.001, URL http://www.sciencedirect.com/science/article/pii/S0968090X1830144X.

Feng, S., Zhang, Y., Li, S.E., Cao, Z., Liu, H.X., Li, L., 2019. String stability for vehicular platoon control: Definitions and analysis methods. Annu. Rev. Control.

Gradinescu, V., Gorgorin, C., Diaconescu, R., Cristea, V., Iftode, L., 2007. Adaptive traffic lights using car-to-car communication. In: IEEE 65th Vehicular Technology Conference. IEEE, Dublin, pp. 21–25. http://dx.doi.org/10.1109/VETECS.2007.17, URL https://ieeexplore.ieee.org/ielx5/4196544/4212428/04212445.pdf?tp=&arnumber=4212445&isnumber=4212428.

Guler, S.I., Menendez, M., Meier, L., 2014. Using connected vehicle technology to improve the efficiency of intersections. Transp. Res. C 46, 121–131. http://dx.doi.org/10.1016/j.trc.2014.05.008.

Guo, Q., Li, L., Ban, X.J., 2019a. Urban traffic signal control with connected and automated vehicles: A survey. Transp. Res. C 101, 313–334. http://dx.doi.org/10.1016/j.trc.2019.01.026, URL http://www.sciencedirect.com/science/article/pii/S0968090X18311641.

Guo, Y., Ma, J., Xiong, C., Li, X., Zhou, F., Hao, W., 2019b. Joint optimization of vehicle trajectories and intersection controllers with connected automated vehicles: Combined dynamic programming and shooting heuristic approach. Transp. Res. C 98, 54–72. http://dx.doi.org/10.1016/j.trc.2018.11.010, URL http://www.sciencedirect.com/science/article/pii/S0968090X18303279.

Gurobi Optimization, Inc., 2019. Gurobi Optimizer Reference Manual. URL http://www.gurobi.com/.

Han, K., Gayah, V.V., 2015. Continuum signalized junction model for dynamic traffic networks: Offset, spillback, and multiple signal phases. Transp. Res. B 77, 213–239. http://dx.doi.org/10.1016/j.trb.2015.03.005, URL http://www.sciencedirect.com/science/article/pii/S019126151500048X.

Han, K., Gayah, V.V., Piccoli, B., Friesz, T.L., Yao, T., 2014. On the continuum approximation of the on-and-off signal control on dynamic traffic networks. Transp. Res. B 61, 73–97. http://dx.doi.org/10.1016/j.trb.2014.01.001, URL http://www.sciencedirect.com/science/article/pii/S0191261514000022.

He, Q., Head, K.L., Ding, J., 2012. PAMSCOD: Platoon-based arterial multi-modal signal control with online data. Transp. Res. C 20 (1), 164–184. http://dx.doi.org/10.1016/j.trc.2011.05.007, URL http://www.sciencedirect.com/science/article/pii/S0968090X11000775.

Heydecker, B., 1992. Sequencing of Traffic Signals. In: Mathematics in Transport Planning and Control, Clarendon Press, Oxford.

Joyoung Lee, B.P., 2012. Development and evaluation of a cooperative vehicle intersection control algorithm under the connected vehicles environment. IEEE Trans. Intell. Transp. Syst. 13 (1), 81–90. http://dx.doi.org/10.1109/TITS.2011.2178836.

Kamal, M.A.S., Mukai, M., Murata, J., Kawabe, T., 2013. Model predictive control of vehicles on urban roads for improved fuel economy. IEEE Trans. Control Syst. Technol. 21 (3), 831–841. http://dx.doi.org/10.1109/TCST.2012.2198478.

Kamalanathsharma, R.K., Rakha, H.A., 2013. Multi-stage dynamic programming algorithm for eco-speed control at traffic signalized intersections. In: 16th International IEEE Conference on Intelligent Transportation Systems. ITSC 2013, pp. 2094–2099. http://dx.doi.org/10.1109/ITSC.2013.6728538.

Keviczky, T., Borrelli, F., Fregene, K., Godbole, D., Balas, G.J., 2007. Decentralized receding horizon control and coordination of autonomous vehicle formations. IEEE Trans. Control Syst. Technol. 16 (1), 19–33.

Khayatian, M., Mehrabian, M., Shrivastava, A., 2018. RIM: Robust intersection management for connected autonomous vehicles. In: 2018 IEEE Real-Time Systems Symposium. RTSS, IEEE, pp. 35–44.

Koonce, P., Rodegerdts, L., Lee, K., Quayle, S., Beaird, S., Braud, C., Bonneson, J., Tarnoff, P., Urbanik, T., 2008. Traffic Signal Timing Manual. Technical Report FHWA-HOP-08-024, Federal Highway Administration, Washington, DC, USA, URL https://rosap.ntl.bts.gov/view/dot/20661.

Krajzewicz, D., Erdmann, J., Behrisch, M., Bieker, L., 2012. Recent development and applications of SUMO - Simulation of Urban MObility. Int. J. Adv. Syst. Meas. 5 (3&4), 128–138.

Kuwata, Y., How, J.P., 2010. Cooperative distributed robust trajectory optimization using receding horizon MILP. IEEE Trans. Control Syst. Technol. 19 (2), 423–431.

Levin, M.W., Boyles, S.D., Patel, R., 2016. Paradoxes of reservation-based intersection controls in traffic networks. Transp. Res. A 90, 14–25. http://dx.doi.org/10.1016/j.tra.2016.05.013, URL http://www.sciencedirect.com/science/article/pii/S0965856416303822.

Li, Z., Chitturi, M.V., Zheng, D., Bill, A.R., Noyce, D.A., 2013. Modeling reservation-based autonomous intersection control in VISSIM. Transp. Res. Rec. J. Transp. Res. Board 2381, 81–90. http://dx.doi.org/10.3141/2381-10.

Li, Z., Elefteriadou, L., Ranka, S., 2014a. Signal control optimization for automated vehicles at isolated signalized intersections. Transp. Res. C 49, 1–18. http://dx.doi.org/10.1016/j.trc.2014.10.001.

Li, L., Wang, F., Jiang, R., Hu, J.-M., Ji, Y., 2010. A new car-following model yielding log-normal type headways distributions. Chin. Phys. B 19 (2), http://dx.doi.org/10.1088/1674-1056/19/2/020513, 020513 (6 pp) car following model;log-normal type headways distributions;vehicles;traffic flow research field;vehicle dynamics;Galton board;time headway distributions;.

Li, L., Wen, D., Yao, D., 2014b. A survey of traffic control with vehicular communications. IEEE Trans. Intell. Transp. Syst. 15 (1), 425–432. http://dx.doi.org/10.1109/TITS.2013.2277737.

Li, Z., Wu, Q., Yu, H., Chen, C., Zhang, G., Tian, Z.Z., Prevedouros, P.D., 2019. Temporal-spatial dimension extension-based intersection control formulation for connected and autonomous vehicle systems. Transp. Res. C 104, 234–248. http://dx.doi.org/10.1016/j.trc.2019.05.003, URL http://www.sciencedirect.com/science/article/pii/S0968090X18305436.

Li, N., Yao, Y., Kolmanovsky, I., Atkins, E., Girard, A.R., 2020. Game-theoretic modeling of multi-vehicle interactions at uncontrolled intersections. IEEE Trans. Intell. Transp. Syst. 23 (2), 1428–1442.

Liang, X.J., Guler, S.I., Gayah, V.V., 2018. Signal timing optimization with connected vehicle technology: platooning to improve computational efficiency. Transp. Res. Rec. 2672 (18), 81–92. http://dx.doi.org/10.1177/0361198118786842.

Little, J.D.C., Kelson, M.D., Gartner, N.H., 1981. MAXBAND: A program for setting signals on arteries and triangular networks. Transp. Res. Rec. J. Transp. Res. Board 795, 40–46.

Liu, R., Smith, M., 2015. Route choice and traffic signal control: A study of the stability and instability of a new dynamical model of route choice and traffic signal control. Transp. Res. B 77, 123–145. http://dx.doi.org/10.1016/j.trb.2015.03.012, URL http://www.sciencedirect.com/science/article/pii/S0191261515000557.

Liu, M., Wang, M., Hoogendoorn, S., 2019. Optimal platoon trajectory planning approach at arterials. Transp. Res. Rec. 0361198119847474.

Lu, G., Shen, Z., Liu, X., Nie, Y.M., Xiong, Z., 2022. Are autonomous vehicles better off without signals at intersections? A comparative computational study. Transp. Res. B 155, 26–46.
Makarem, L., Gillet, D., 2012. Fluent coordination of autonomous vehicles at intersections. In: 2012 IEEE International Conference on Systems, Man, and Cybernetics. SMC, IEEE, pp. 2557–2562.
Malikopoulos, A.A., Cassandras, C.G., Zhang, Y.J., 2018. A decentralized energy-optimal control framework for connected automated vehicles at signal-free intersections. Automatica 93, 244–256. http://dx.doi.org/10.1016/j.automatica.2018.03.056.
Memoli, S., Cantarella, G.E., de Luca, S., Pace, R.D., 2017. Network signal setting design with stage sequence optimisation. Transp. Res. B 100, 20–42. http://dx.doi.org/10.1016/j.trb.2017.01.013, URL http://www.sciencedirect.com/science/article/pii/S0191261516302363.
Mirheli, A., Tajalli, M., Hajibabai, L., Hajbabaie, A., 2019. A consensus-based distributed trajectory control in a signal-free intersection. Transp. Res. C 100, 161–176. http://dx.doi.org/10.1016/j.trc.2019.01.004, URL http://www.sciencedirect.com/science/article/pii/S0968090X18311343.
Mitrovic, N., Dakic, I., Stevanovic, A., 2020. Combined alternate-direction lane assignment and reservation-based intersection control. IEEE Trans. Intell. Transp. Syst. 21 (4), 1779–1789.
Mohajerpoor, R., Saberi, M., Ramezani, M., 2019. Analytical derivation of the optimal traffic signal timing: Minimizing delay variability and spillback probability for undersaturated intersections. Transp. Res. B 119, 45–68. http://dx.doi.org/10.1016/j.trb.2018.11.004, URL http://www.sciencedirect.com/science/article/pii/S0191261518300201.
Mohebifard, R., Hajbabaie, A., 2019. Optimal network-level traffic signal control: A benders decomposition-based solution algorithm. Transp. Res. B 121, 252–274. http://dx.doi.org/10.1016/j.trb.2019.01.012, URL http://www.sciencedirect.com/science/article/pii/S0191261518307616.
Newell, G.F., 2002. A simplified car-following theory: a lower order model. Transp. Res. B 36 (3), 195–205. http://dx.doi.org/10.1016/S0191-2615(00)00044-8, URL http://www.sciencedirect.com/science/article/pii/S0191261500000448.
Papageorgiou, M., Diakaki, C., Dinopoulou, V., Kotsialos, A., Wang, Y., 2003. Review of road traffic control strategies. Proc. IEEE 91 (12), 2043–2067. http://dx.doi.org/10.1109/JPROC.2003.819610.
Pei, H., Feng, S., Zhang, Y., Yao, D., 2019. A cooperative driving strategy for merging at on-ramps based on dynamic programming. IEEE Trans. Veh. Technol..
Qian, B., Zhou, H., Lyu, F., Li, J., Ma, T., Hou, F., 2019. Toward collision-free and efficient coordination for automated vehicles at unsignalized intersection. IEEE Internet Things J. 6 (6), 10408–10420.
Randriamasy, M., Cabani, A., Chafouk, H., Fremont, G., 2019. Geolocation process to perform the electronic toll collection using the ITS-G5 technology. IEEE Trans. Veh. Technol. 68 (9), 8570–8582.
Shahidi, N., Au, T.C., Stone, P., 2011. Batch reservations in autonomous intersection management. In: The 10th International Conference on Autonomous Agents and Multiagent Systems-Volume 3. Citeseer, pp. 1225–1226.
Sun, C., Guanetti, J., Borrelli, F., Moura, S.J., 2020. Optimal eco-driving control of connected and autonomous vehicles through signalized intersections. IEEE Internet Things J. 7 (5), 3759–3773.
Sun, W., Zheng, J., Liu, H.X., 2017. A capacity maximization scheme for intersection management with automated vehicles. Transp. Res. C 23, 121–136.
Tachet, R., Santi, P., D Sobolevsky, S., Reyes-Castro, L.I., Frazzoli, E., Helbing, D., Ratti, C., 2016. Revisiting street intersections using slot-based systems. PLoS One 11 (3), 1–9. http://dx.doi.org/10.1371/journal.pone.0149607.
Transportation Research Board (TRB), 2010. HCM 2010: Highway Capacity Manual. Transportation Research Board, Washington, D.C..
Ubiergo, G.A., Jin, W.L., 2016. Mobility and environment improvement of signalized networks through Vehicle-to-Infrastructure (V2I) communications. Transp. Res. C 68, 70–82. http://dx.doi.org/10.1016/j.trc.2016.03.010, URL http://www.sciencedirect.com/science/article/pii/S0968090X16300031.
Wan, N., Vahidi, A., Luckow, A., 2016. Optimal speed advisory for connected vehicles in arterial roads and the impact on mixed traffic. Transp. Res. C 69, 548–563. http://dx.doi.org/10.1016/j.trc.2016.01.011, URL http://www.sciencedirect.com/science/article/pii/S0968090X16000292.
Wang, M., Daamen, W., Hoogendoorn, S.P., van Arem, B., 2014a. Rolling horizon control framework for driver assistance systems. Part I: Mathematical formulation and non-cooperative systems. Transp. Res. C 40, 271–289. http://dx.doi.org/10.1016/j.trc.2013.11.023, URL http://www.sciencedirect.com/science/article/pii/S0968090X13002593.
Wang, M., Daamen, W., Hoogendoorn, S.P., van Arem, B., 2014b. Rolling horizon control framework for driver assistance systems. Part II: Cooperative sensing and cooperative control. Transp. Res. C 40, 290–311. http://dx.doi.org/10.1016/j.trc.2013.11.024, URL http://www.sciencedirect.com/science/article/pii/S0968090X13002611.
Webster, F.V., 1958. Traffic Signal Settings. In: Road Research Technical Paper, vol. 39, Her Majesty's Stationery Office, London, England.
Xu, B., Li, S.E., Bian, Y., Li, S., Ban, X.J., Wang, J., Li, K., 2018. Distributed conflict-free cooperation for multiple connected vehicles at unsignalized intersections. Transp. Res. C 93, 322–334. http://dx.doi.org/10.1016/j.trc.2018.06.004, URL http://www.sciencedirect.com/science/article/pii/S0968090X18308246.
Yang, K., Zheng, N., Menendez, M., 2017. Multi-scale perimeter control approach in a connected-vehicle environment. Transp. Res. Procedia 23, 101–120. http://dx.doi.org/10.1016/j.trpro.2017.05.007, URL http://www.sciencedirect.com/science/article/pii/S2352146517302843, Papers Selected for the 22nd International Symposium on Transportation and Traffic Theory Chicago, Illinois, USA, 24-26 July, 2017.
Yao, Z., Jiang, H., Cheng, Y., Jiang, Y., Ran, B., 2020. Integrated schedule and trajectory optimization for connected automated vehicles in a conflict zone. IEEE Trans. Intell. Transp. Syst. 1–11. http://dx.doi.org/10.1109/TITS.2020.3027731.
Yu, C., Feng, Y., Liu, H.X., Ma, W., Yang, X., 2018. Integrated optimization of traffic signals and vehicle trajectories at isolated urban intersections. Transp. Res. B 112, 89–112. http://dx.doi.org/10.1016/j.trb.2018.04.007, URL https://www.sciencedirect.com/science/article/pii/S0191261517306215.
Yu, C., Feng, Y., Liu, H.X., Ma, W., Yang, X., 2019a. Corridor level cooperative trajectory optimization with connected and automated vehicles. Transp. Res. C 105, 405–421. http://dx.doi.org/10.1016/j.trc.2019.06.002, URL http://www.sciencedirect.com/science/article/pii/S0968090X18316103.
Yu, C., Sun, W., Liu, H.X., Yang, X., 2019b. Managing connected and automated vehicles at isolated intersections: From reservation- to optimization-based methods. Transp. Res. B 122, 416–435. http://dx.doi.org/10.1016/j.trb.2019.03.002, URL http://www.sciencedirect.com/science/article/pii/S0191261517309980.
Zhang, Y.J., Malikopoulos, A.A., Cassandras, C.G., 2016. Optimal control and coordination of connected and automated vehicles at urban traffic intersections. In: 2016 American Control Conference. ACC, IEEE, pp. 6227–6232.
Zhong, H.S., Wang, H., Deng, Y.H., Chen, M.C., Peng, L.C., Luo, Y.H., Qin, J., Wu, D., Ding, X., Hu, Y., Hu, P., Yang, X.Y., Zhang, W.J., Li, H., Li, Y., Jiang, X., Gan, L., Yang, G., You, L., Wang, Z., Li, L., Liu, N.L., Lu, C.Y., Pan, J.W., 2020. Quantum computational advantage using photons. Science 370 (6523), 1460–1463. http://dx.doi.org/10.1126/science.abe8770, URL https://www.science.org/doi/abs/10.1126/science.abe8770. arXiv:https://www.science.org/doi/pdf/10.1126/science.abe8770.
Zohdy, I.H., Rakha, H.A., 2016. Intersection management via vehicle connectivity: The intersection cooperative adaptive cruise control system concept. J. Intell. Transp. Syst. 20 (1), 17–32. http://dx.doi.org/10.1080/15472450.2014.889918.